Rgs1 is a regulator of effector gene expression during plant infection by the rice blast fungus *Magnaporthe oryzae*

Bozeng Tang[a], Xia Yan[a], Lauren S. Ryder[a], Neftaly Cruz-Mireles[a], Darren M. Soanes[b], Camilla Molinari [a], Andrew J. Foster[a], and Nicholas J. Talbot[a]

[a]The Sainsbury Laboratory, University of East Anglia, Norwich Research Park, NR4 7UH, United Kingdom;
[b]School of Biosciences, University of Exeter, Exeter, EX4 4QD, United Kingdom.

* To whom correspondence should be addressed
Email: nick.talbot@tsl.ac.uk

Bozeng Tang, https://orcid.org/0000-0002-3986-9622

Xia Yan, https://orcid.org/0000-0003-4509-0137

Lauren S. Ryder, https://orcid.org/0000-0003-0370-5746

Neftaly C. Mireles, http://orcid.org/0000-0003-1031-1470

Darren M. Soanes, https://orcid.org/0000-0001-5025-295X

Camilla Molinari, https://orcid.org/0000-0003-0059-186X

Andy J. Foster http://orcid.org/0000-0002-8459-7590

Nicholas J. Talbot, https://orcid.org/0000-0001-6434-7757

Classification
BIOLOGICAL SCIENCES: Agricultural Sciences

Keywords
Plant pathogen, effectors, rice blast, gene expression

Abstract

To cause rice blast disease the filamentous fungus *Magnaporthe oryzae* secretes a battery of effector proteins into host plant tissue to facilitate infection. Effector-encoding genes are expressed only during plant infection and show very low expression during other developmental stages. How effector gene expression is regulated in such a precise manner during invasive growth by *M. oryzae* is not known. Here, we report a forward-genetic screen to identify regulators of effector gene expression, based on selection of mutants that show constitutive effector gene expression. Using this simple screen, we identify Rgs1, a regulator of G-protein signalling (RGS) protein that is necessary for appressorium development, as a novel transcriptional regulator of effector gene expression, which acts prior to plant infection. We show that an N-terminal domain of Rgs1, possessing transactivation activity, is required for effector gene regulation and acts in an RGS-independent manner. Rgs1 controls expression of at least 60 temporally co-regulated effector genes, preventing their transcription during the pre-penetration stage of development prior to plant infection. A regulator of appressorium morphogenesis is therefore also required for orchestration of pathogen gene expression required for invasive growth by *M. oryzae* during plant infection.

Introduction

Plant pathogens secrete effector proteins into host tissues in order to suppress host immunity, modulate plant cell organisation and perturb cellular functions (1, 2). In this way, they re-programme host cells to facilitate pathogen invasion and proliferation. Effector gene expression is tightly regulated so that different families of effectors are deployed at each stage of plant infection. How plant pathogenic fungi regulate effector gene expression is, however, poorly understood. This is exemplified by the devastating rice blast pathogen *Magnaporthe oryzae* which possesses a large repertoire of effector genes expressed specifically during plant cell invasion (3). Although the function of effectors is an area of intense study (4), relatively little is known about the transcriptional control that governs effector gene expression (5-8).

In this study, we set out to investigate transcriptional regulation of effector-encoding genes in *M. oryzae* and how gene expression is orchestrated during plant infection. On the leaf surface, *M. oryzae* conidia germinate and sense plant surface cues which trigger development of a specialised infection cell, the appressorium, required for penetration of host cells (9-11). Appressorium development requires heterotrimeric G-protein signalling, to transmit surface-sensing cues to downstream modules that facilitate morphogenesis, controlled by the mitogen-activated protein kinase Pmk1 (12, 13), and cAMP-dependent protein kinase A pathways (14). G-protein subunits in *M. oryzae* are controlled by Regulator of G-protein Signalling (RGS) proteins, which are important for appressorium development (15-17).

After penetration into rice tissue, the blast fungus rapidly switches to biotrophic growth and overcomes plant immunity by secreting effector proteins (18). At the tip of the primary invasive hypha, a plant-derived membrane-rich structure, the Biotrophic Interfacial Complex (BIC), develops and remains intact as further secondary invasive hyphae fill the rice cell (19). Effectors of *M. oryzae* destined for delivery into plant cells, including avirulence gene products such as Avr-Pita, Avr-Pizt, Avr-Pii and Pwl2, all localize to the BIC (20, 21), from which they appear to be translocated and delivered into host cells (5). A second group of effectors, including Slp1 and Bas4, are secreted to the apoplast where they suppress extracellular defence responses, such as chitin-triggered immunity (22). As a consequence of effector-mediated suppression of immunity, *M. oryzae* is able to proliferate rapidly in plant tissue and move from cell-to-cell using pit fields containing plasmodesmata. The fungus develops a specialised transpressorium at rice cell junctions, which facilitates cell invasion at pit fields in a process regulated by the Pmk1 MAPK pathway (23).

A recent transcriptional profiling study has shown that effector gene expression in *M. oryzae* occurs only during plant infection. Effector genes are temporally regulated during infection with early-acting effectors expressed as soon as 8 hours after conidial germination, and large families of structurally conserved effectors, such as the Max effectors (24), expressed during biotrophic growth of the pathogen, 24-48 hours after initial infection (25). The specific temporal and

69 spatial expression patterns suggest that *M. oryzae* effectors must be under very precise
70 transcriptional regulation, but little is known regarding the transcriptional regulators necessary to
71 achieve this complexity of control. In other pathogenic fungi, our understanding of effector gene
72 regulation is also limited. In the corn smut fungus *Ustilago maydis*, for instance, a transcriptional
73 regulator Ros1 has been implicated in spore formation and effector gene expression during the late
74 stages of infection (26), while in the necrotrophic wheat pathogen *Parastagonospora nodorum* the
75 Zn_2Cys_6 transcription factor PnPf2 positively regulates 12 effector-like protein-encoding genes (27).
76 Recent studies have also implicated global histone modification dynamics in control of pathogen
77 gene expression in *M. oryzae* during infection (28). There are, however, only limited reports to date
78 that have investigated the mechanism of effector gene regulation in plant pathogenic fungi.
79 In this study, we set out to identify putative regulators of effector gene expression. We
80 reasoned that because effector genes are only expressed during growth in plant tissue, it would be
81 possible to select for mutants that exhibit constitutive effector gene expression. These would
82 potentially carry mutations in genes encoding transcriptional regulators. Here, we report a simple
83 forward genetic screen using a strain of *M. oryzae* in which we expressed a translational fusion of
84 an effector, Mep2, with a green fluorescent protein tag. Using this reporter line, we selected *M.*
85 *oryzae* mutants in which we could observe constitutive Mep2-GFP fluorescence in hyphae and
86 spores. This led to identification of a mutant, *cer7*, which carries a single point mutation in a gene
87 called *RGS1*. We show that the Rgs1 protein– which has been previously implicated as a regulator
88 of G-protein signalling during appressorium development by *M. oryzae* (15-17) –also acts as a
89 transcriptional regulator of effector gene expression. We provide evidence that Rgs1 is necessary
90 for repressing the expression of at least 60 temporally co-regulated effector-encoding genes during
91 the pre-penetration stages of development and that these genes are subsequently de-repressed
92 during invasive growth by the fungus enabling their specific deployment in plant tissue.
93
94 **Results**
95
96 **A forward genetic screen to identify regulators of effector gene expression in *M. oryzae*.**
97 In this study, we set out to identify transcriptional regulators of effector gene expression in *M.*
98 *oryzae*. We reasoned that because effectors are only expressed during plant infection, selecting
99 mutants that show constitutive expression of an effector gene, would provide a simple method to
100 identify corresponding regulatory gene, carrying either a mutation leading to constitutive activation
101 of a transcriptional activator, or a loss of function mutation in a repressor, for example. We therefore
102 generated a strain of *M. oryzae* expressing an effector-encoding gene *MEP2*, fused to the Green
103 Fluorescent Protein gene (GFP). *MEP2* was identified in a recent study that characterised the
104 effector repertoire of *M. oryzae* based on their differential expression during pathogenesis (25).
105 *MEP2* shows peak expression 48h after infection based on RNA-seq analysis, corresponding to a

106 time of rapid plant tissue biotrophic colonisation by the fungus (25). We generated a *MEP2:GFP*
107 gene fusion, transformed it into a *M. oryzae* wild type rice pathogenic strain Guy11 and selected a
108 transformant with a single integration of the reporter gene construct. We observed specific
109 expression and localisation of Mep2-GFP fluorescence in the Biotrophic Interfacial Complex (BIC)
110 of invasive hyphae during rice infection, with very little detectable expression in either conidia or
111 vegetative hyphae of the fungus (Fig. 1*A,* Fig S1). Consistent with this, quantitative real-time PCR
112 (qPCR) showed high transcript abundance of *MEP2* in invasive hyphae (IH) with peak expression
113 at 48 h post-inoculation (hpi) compared to minimal basal expression in conidia (Fig. 1*B*). Having
114 established that Mep2-GFP is specifically expressed during *in planta* growth by *M. oryzae*, we
115 carried out UV mutagenesis on conidia of the Mep2-GFP strain. We selected mutants that showed
116 constitutive Mep2-GFP fluorescence in conidia and named them Cer (Constitutive Effector
117 Regulator) mutants. One of these mutants, *cer7,* which has green fluorescent conidia, was selected
118 (Fig. 1*C*). We verified constitutive expression of *MEP2* using qPCR which showed elevated
119 expression in *cer7*, compared to the original Mep2-GFP transformant (Fig. 1*D*). We also observed
120 constitutive expression of Mep2-GFP in mycelium grown in axenic culture, in appressoria, and in
121 the BIC of invasive hyphae in the *cer7* mutant (*SI Appendix*, Fig. S1). Taken together, these results
122 suggest that the expression of the *MEP2* effector gene is induced, or de-repressed in spores and
123 mycelium of the *cer7* mutant.
124
125 **Identification of the *CER7* locus by bulked segregant analysis**
126 To identify the mutation leading to constitutive *MEP2* expression in the *cer7* mutant we first
127 sequenced the genome of *cer7* mutant and aligned it against the genome sequence of the original
128 Guy11 Mep2-GFP transformant and the *M. oryzae* reference genome of strain 70-15 (29). A total
129 of 1955 variants (SNPs and indels) were identified compared to the *M. oryzae* 70-15 reference
130 genome sequence of which 1036 were located within the coding regions of 408 different genes. To
131 identify the *cer7* mutation, we carried out bulked segregant analysis (30) by crossing the *cer7*
132 (*Mat1-1*) mutant with a wild-type strain TH3 of opposite mating type (*Mat1-2*) (*SI Appendix*, Fig.
133 S2*A*). We selected perithecia and dissected asci (*SI Appendix*, Fig. S2*B*). Ascospore progeny were
134 then collected and phenotypically characterized based on the fluorescence signal of Mep2-GFP
135 (Fig. 2*A*). A total of 253 progeny were selected, of which 59 progeny (23.3%) showed the *cer7*
136 phenotype, and 194 progeny the wild type phenotype (Fig. 2*A*). The *MEP2-GFP* construct is
137 present in a single copy in the *cer7* mutant, as confirmed by *de novo* assembly of the *cer7* genome
138 sequence and would therefore be predicted to segregate in a 1:1 ratio in ascospore progeny. We
139 reasoned that if *cer7* is caused by mutation at a single locus then this should also segregate in a
140 1:1 ratio. We would therefore expect to see the observable *cer7* fluorescent conidia phenotype in
141 a 1:3 ratio, with a quarter of progeny showing constitutive Mep2-GFP expression, which was
142 validated by a Chi-squared test (χ^2 = 0.135, df=1, P = 0.713). To carry out bulked segregant

143 analysis we then extracted genomic DNA from *cer7* and wild-type progeny, respectively, and bulked
144 them into two separate pools for genome sequencing. This enabled us to define a region of 692kb
145 on supercontig 8.2 which showed the highest frequency of SNPs identified in progeny showing the
146 *cer7* phenotype (Fig. 2*B*). Within this region, only one polymorphism matched SNPs identified in
147 the genome sequence of the *cer7* mutant, located at position 3779156 in the coding region of gene
148 MGG_14517. This gene has previously been identified as *RGS1*, which encodes a regulator of G-
149 protein signalling in *M. oryzae* (15). The SNP results in a single amino acid sequence change in
150 the predicted gene product from glutamic acid to a stop codon (GAA to TAA) (*SI Appendix*, Fig.
151 S2*C*). To confirm the association, we sequenced PCR-amplified fragments spanning the SNP in
152 10 *cer7* and 10 wild type progeny (*SI Appendix*, Fig. S2*D*), which verified the analysis.
153 To test whether the *RGS1* gene corresponds to *cer7* we carried out genetic
154 complementation and allelic replacement assays. We first introduced the wild type $RGS1^{WT}$ allele
155 into the *cer7* mutant, which resulted in transformants with non-fluorescent conidia (Fig. 2*C*).
156 Introducing the $rgs1^{cer7}$ allele ectopically into the wild-type ($RGS1^{+}$) Mep2-GFP strain also resulted
157 in non-fluorescent conidia. By contrast, when we carried out targeted allelic replacement of *RGS1*
158 with the $rgs1^{cer7}$ mutant allele in the Mep2-GFP strain, this resulted in transformants with fluorescent
159 conidia. When considered together, this provides evidence that *cer7* is a recessive loss of function
160 mutation in the *RGS1* gene, consistent with the premature stop codon generated by the mutation
161 (Fig. 2*C*). To test this idea directly, we generated a targeted gene deletion mutant in the wild type
162 Mep2-GFP background. This led to constitutive expression of Mep2-GFP in conidia of the resulting
163 Δ*rgs1* mutants (Fig. 2*C*). The results were validated by qPCR which confirmed that *cer7* and Δ*rgs1*
164 mutants show high level expression of *MEP2* in conidia (*SI Appendix*, Fig. S3*A*). We also observed
165 the Δ*rgs1* and *cer7* strains produced similar phenotypes in axenic culture, showing white aerial
166 hyphal growth, water soaking, and aberrant appressorium formation on hydrophilic surfaces, which
167 is consistent with previous reports of Δ*rgs1* mutants (15, 16, 31) (*SI Appendix*, Fig. S3*B*).
168
169 **Rgs1 acts as a transcriptional regulator of the *MEP2* effector gene**
170 Rgs1 has been studied previously in *M. oryzae* as a regulator of G-protein signalling which affects
171 asexual development, appressorium formation, surface sensing, and virulence through its
172 interaction with the three Gα subunit proteins MagA, MagB and MagC (15). Mutants lacking Rgs1
173 form appressoria on non-inductive hydrophilic surfaces and show reduced virulence resulting from
174 mis-regulation of MagA, as well as a hyper-sporulation phenotype associated with mis-regulation
175 of MagB (31). The reported roles of Rgs1 are therefore associated with the pre-penetration phase
176 of development, prior to plant tissue invasion (16, 17, 31). To investigate the potential role of Rgs1
177 as an effector regulator, we therefore investigated the temporal expression of *RGS1* in publicly
178 available RNA-seq data-set (PRJEB45007) (25). This showed that *RGS1* is expressed in conidia
179 and during initial stages of appressorium formation, but then very reduced in expression during

180 plant infection. This is the reciprocal pattern to *MEP2*, which is not expressed in conidia, but highly
181 expressed during invasive growth, peaking in expression at 48h after infection (Fig. 3*A*). To
182 experimentally verify this pattern of expression, we generated a *M. oryzae* transformant expressing
183 Rgs1-GFP and carried out live cell imaging. Rgs1-GFP is highly expressed in conidia, germ tubes,
184 and incipient appressoria, but significantly reduced in invasive hyphae (Fig. 3*B*). We then extracted
185 total protein from mycelium and plant tissue infected with the Rgs1-GFP strain, and a control strain
186 of *M. oryzae* expressing GFP under control of a high-level constitutive promoter ToxA (32), and
187 performed western blot analysis with anti-GFP antibodies. We detected the predicted 106 kDa
188 Rgs1-GFP fusion protein in mycelium, but this was not observed in infected plant tissue samples
189 at 32h after infection (*SI Appendix*, Fig. S4*A*). To investigate the nature of Rgs1 expression further,
190 we next analysed published RNA-seq data (PRJEB36580)(33), and found high coverage reads
191 spanning all three exons of *RGS1* from conidia, while aligned reads from the first exon of *RGS1*
192 were very reduced in RNA-seq data from infected plant material at 24 hpi (*SI Appendix*, Fig. S4*B*).
193 This suggests that exon skipping of *RGS1* may occur during plant infection, resulting in a lower
194 abundance of the N-terminal domain of the Rgs1 protein. It has previously been reported that Rgs1
195 undergoes endoproteolytic cleavage which leads to generation of a tandem Dishevelled, Egl-10,
196 Pleckstrin domain (DEP-DEP) protein from the N-terminus of Rgs1 (N-Rgs1), encoded by the first
197 and second exon, and a separate RGS core domain protein from the C-terminus (C-Rgs1) (31). It
198 has been proposed that the N-Rgs1 protein is required for vesicular membrane targeting of the
199 protein, while the C-Rgs1 protein is sequestered in the vacuole, providing a post-translational
200 mechanism to regulate the catalytic activity of Rgs1 on its Gα sub-unit substrates. Given the low
201 level of N-Rgs1 associated transcripts during plant infection, we wondered whether the effector
202 regulation function resided in N-Rgs1 and occurred during the pre-penetration phases of
203 development. To investigate whether N-Rgs1 can act as a transcription factor, we therefore tested
204 its transactivation activity and DNA-binding ability in yeast. We found that when N-Rgs1 is fused to
205 the Gal4 DNA-binding domain it is able to act as a transcriptional activator (Fig. 3*C*), but when
206 fused to the Gal4 activation domain, it is unable to bind DNA (*SI Appendix*, Fig. S5*A*). Meanwhile,
207 neither the full length Rgs1 nor the C-Rgs1 protein show any transactivation or DNA-binding activity
208 (*SI Appendix*, Fig. S5*A*). These results suggest that N-Rgs1 might function independently to
209 regulate *MEP2* transcription, consistent with the position of the *cer7* premature stop codon mutation
210 and the potential that exon skipping of Rgs1 takes place during plant infection. To test this idea,
211 we constructed vectors carrying sequences encoding N-Rgs1 or C-Rgs1 respectively, driven by
212 the native *RGS1* promoter and terminator sequences, and transformed these into the *M. oryzae*
213 *cer7* mutant. We found that N-Rgs1 was able to complement *cer7* preventing expression of Mep2-
214 GFP in conidia (Fig. 3*D*). By contrast, expressing C-Rgs1 did not complement the *cer7* phenotype
215 and conidia remained fluorescent (Fig. 3*D*). In control experiments we verified *cer7*
216 complementation with the full-length *RGS1* gene and lack of complementation with the $RGS1^{cer7}$

217 allele. When considered together, these results suggest that N-Rgs1 acts as a repressor of
218 transcription of *MEP2* in conidia, preventing its expression prior to plant infection. However, given
219 that N-Rgs1 is unable to bind DNA, which was also confirmed using a yeast-one hybrid assay which
220 did not find any evidence for N-Rgs1 binding to the *MEP2* promoter (*SI Appendix*, Fig. S5*B*), it is
221 likely that N-Rgs1 regulates transcription of *MEP2* indirectly, perhaps by activating a repressor
222 protein, or acting in association with another partner to bring about *MEP2* repression. We conclude
223 that N-Rgs1 is necessary for regulation of the *MEP2* effector gene.
224
225 **Rgs1 regulates effector gene expression independently of its G-protein signalling function**
226 Rgs1 has been reported to accelerate the intrinsic GTPase activity of target Gα subunits during
227 appressorium development (15) and we therefore decided to test directly whether its RGS activity,
228 which resides in the C-Rgs1 part of the protein, was associated with its ability to regulate *MEP2*
229 transcription. We decided to test whether repression of *MEP2* transcription during the pre-
230 penetration stage of development is regulated via the action of Rgs1 on its associated Gα-subunits
231 in response to surface cues, thereby enabling Gα subunits to activate their downstream effector
232 modules to trigger *MEP2* transcription. We reasoned that if *MEP2* transcription is G-protein-
233 dependent, then mutants affected in their sensitivity to Rgs1 signalling, lacking GTPase activity, or
234 constitutively activated GTP-Gα-subunits, would be affected in *MEP2* transcription. To test this
235 idea, we generated Rgs1-insensitive alleles MagA(G187S), MagB(G183S), and MagC(G184S), the
236 GTP-ase inactive MagA(Q208L) and MagB(Q204L) alleles, and the MagB(G42R) constitutively
237 activated allele (15), and introduced them each into the Guy11 strain expressing Mep2-GFP. We
238 did not observe increased Mep2-GFP expression in conidia of any of these transformants,
239 suggesting that Rgs1 regulates transcription of *MEP2* in a G-protein-independent manner (*SI*
240 *Appendix*, Fig. S5*C*). Taken together, these results provide evidence that the N-Rgs1 protein is
241 necessary to regulate transcription of *MEP2* in conidia and acts independently of the G-protein
242 signalling role of Rgs1.
243
244 **Rgs1 regulates a large group of effector genes in *M. oryzae***
245 To determine the wider function of Rgs1 we tested the ability of the Δ*rgs1* and *cer7* mutants to
246 cause rice blast disease. We inoculated 21-day-old seedlings of the susceptible rice cultivar CO-
247 39 and scored disease symptoms after 5 days. A significant reduction in disease lesion number
248 was observed in Δ*rgs1* and *cer7* infections compared to the isogenic wild type Guy11 (Fig. 4*A*).
249 Rgs1 has previously been reported to play a role in pathogenesis, but this has been attributed to
250 its G-protein regulatory function (11). We decided to test whether Rgs1 regulates a wider group of
251 virulence-associated genes by performing comparative global transcriptional profiling using Δ*rgs1*
252 and *cer7* mutants compared to Guy11. We reasoned that genes regulated by Rgs1 during plant
253 infection would show a similar de-repression in conidia of Δ*rgs1* and *cer7* mutants. We therefore

254 extracted mRNA from conidia Δ*rgs1*, *cer7*, and Guy11 using a total of five biological replicates of
255 the experiment and performed RNA-seq analysis. Euclidean analysis was used to determine the
256 similarity between expression profiles in each mutant, revealing a strong overlap between Δ*rgs1*
257 and *cer7* mutants (Fig. 4*B*). This was consistent with principal component analysis which also
258 demonstrated very similar transcriptional patterns between the *cer7* and Δ*rgs1* mutant (*SI*
259 *Appendix*, Fig. S6*A*). In total, 996 genes were upregulated in conidia of *cer7*, and 1126 in Δ*rgs1*
260 compared to Guy11 (log2|FC|>1, padj<0.05). Of these, 757 are shared between *cer7* and Δ*rgs1*.
261 Metabolic enrichment analysis of the Rgs1-repressed gene set showed over-representation of
262 gene functions associated with starch and sucrose metabolism, and glycan degradation, which are
263 also induced during biotrophic invasive fungal growth, as well as phenylalanine and tyrosine
264 metabolism which may be associated with secondary metabolism (*SI Appendix*, Fig. S6*B*). We also
265 observed over-representation of biological processes associated with membrane function and
266 transmembrane transport, as well as oxido-reductases. These functions too are associated with
267 biotrophic invasive growth of *M. oryzae* (25) (*SI Appendix*, Fig. S6*C*). A recent study of the
268 transcriptional landscape of plant infection by *M. oryzae* used weighted gene co-expression
269 network analysis (WCGNA) to define temporal co-expression clusters of *M. oryzae* genes during
270 infection (25) (*SI Appendix*, Fig. S7*A*). We observed that Rgs1-regulated genes can be classified
271 into each WCGNA cluster but genes upregulated in conidia of Δ*rgs1* mutants are enriched in cluster
272 M5, which peaks in expression at 48 h after infection (*SI Appendix*, Fig. S7*A*). This cluster also
273 contains many effector-encoding genes (25). Consistent with this, we found 98 predicted or known
274 effector-encoding genes upregulated in conidia of Δ*rgs1* mutants, of which 60 were also up-
275 regulated in conidia of the *cer7* mutant (Fig. 4*C*) (*SI Appendix*, table S3). This suggests that in
276 addition to *MEP2*, Rgs1 may regulate a much larger group of effectors, that are de-repressed in
277 conidia when the function of Rgs1 is compromised. Among this group, there were 8 previously
278 reported effector candidates, including *BAS3*, *BAS113*, *MEP19*, and *MEP27* (8, 25), and the
279 necrosis and ethylene-inducing (Nep-like) peptide effector *NLP4* which is involved in programmed
280 cell death in plant tissue (34) (Fig. 4*D*). To test whether the identified effectors are also de-
281 repressed in a *cer7* mutant we generated *BAS113-RFP* and *BAS3-RFP* gene fusions and
282 transformed them into the *cer7* mutant strain and Guy11, respectively. We observed high levels of
283 Bas3-RFP and Bas113-RFP fluorescence in conidia of the *cer7* mutant transformants, compared
284 to Guy11 (Fig. 4*E*), which provides further evidence that Rgs1 regulates additional effectors to
285 Mep2. Transcriptional profile analysis of the 60 putatively Rgs1-repressed effectors during infection
286 demonstrated that they peak in expression 48 and 72hpi (*SI Appendix*, Fig. S7*B*).
287
288 **Rgs1 contributes to pathogen fitness during rice blast disease**
289 Given that Rgs1 potentially regulates the expression of a large group of effectors, we decided to
290 investigate the biological significance of the effector regulation mediated by Rgs1. When we

291 inoculated rice leaf sheath with conidia of Δ*rgs1*, we found that invasive hyphae grew more slowly
292 than those of Guy11 (Fig. 5*A*). We therefore tested whether this reduced growth in plant tissue was
293 a consequence of the mis-regulation of effector gene expression. As many effectors act to suppress
294 plant defence, we performed a qPCR experiment to investigate expression of a sub-set of defence-
295 related rice genes from leaf sheath samples following infection by Guy11 and Δ*rgs1*, respectively.
296 Transcripts of rice *PR1a* (35) and *CPS2* (36), are induced significantly at 16hpi and at 24hpi in rice
297 tissue inoculated by strain Δ*rgs1*, compared to infection with Guy11 or non-infected tissue (Fig.
298 5*B*). These results are consistent with Rgs1 being required for the correct temporal dynamics of
299 effector gene expression. However, we recognised that the role of Rgs1 was most likely to be
300 involved in repressing effector gene expression prior to plant infection. We therefore decided to
301 investigate the consequence of over-expressing *RGS1* throughout plant infection. For this we
302 generated a ToxAp*:RGS1* construct and introduced it into the Mep2-GFP background. Over-
303 expression of Rgs1 led to complete repression of Mep2-GFP during invasive growth with no visible
304 BIC localisation observed in Guy11 (*SI Appendix*, Fig. S8). We then tested the ability of the
305 *ToxAp:RGS1* strain to cause rice blast disease (Fig. 5*C*). We did not find a clear reduction in
306 disease symptoms in lesion density so we decided to use a recently described relative fitness assay
307 to evaluate the effect of over-expressing Rgs1 (25). For this, we used a mixed spore inoculum of
308 the *ToxAp:Rgs1-GFP* strain and a wild type Guy11 strain expressing H1-RFP. The fluorescent
309 markers are simply used as a means of visually distinguishing conidia of each strain. Conidia were
310 mixed in a 1:1 ratio and used to inoculate CO-39 seedlings (Fig. 5*D*). We allowed disease
311 symptoms to develop and then recovered conidia from lesions. We recorded the ratio of each spore
312 type (green or with red nuclei, respectively) recovered from disease lesions and then carried out a
313 second round of infection using the same ratio. We observed that the proportion of *ToxAp:RGS1*
314 conidia reduced after two generations of infection to 30.83% and showed a fitness coefficient of
315 0.45 after two generations (Fig. 5*E*). We conclude that over-expression of *RGS1* has an important
316 fitness consequence for *M. oryzae* consistent with its action as a transcriptional regulator of genes
317 associated with biotrophic fungal growth.
318
319 **Discussion**
320 One of the hallmarks of fungal effector proteins is that they are expressed specifically during
321 pathogenesis. Indeed, one of the main strategies for identifying putative effector candidates has
322 been to use transcriptional profiling to identify differentially expressed pathogen genes. This has
323 revealed the presence of temporally co-expressed families of effector genes in many fungal
324 pathogens including *Ustilago maydis* (37) and *M. oryzae* (25). In rice blast, a very large repertoire
325 of 546 effector genes has been reported, which are temporally co-expressed throughout invasive
326 growth between 8h and 144h after infection, with large families of structurally-related effectors co-
327 expressed between 24h and 48h after infection during biotrophic proliferation of the fungus in rice

328 tissue (25). The complexity of the spatio-temporal regulation of effector gene expression– in which
329 cytoplasmic effectors localise specifically at the BIC during invasive hyphal growth –suggests that
330 sophisticated transcriptional regulation must be present to ensure that effectors are produced and
331 deployed at the correct time and in the correct cells. But even though effectors have been studied
332 intensively in *M. oryzae*, leading to new insight into their host targets and structure-function
333 relationships (38, 39), very little is known about effector gene regulation. In contrast to bacterial
334 pathogens, where effector gene regulation is well understood and associated with co-ordinate
335 operon-based gene control (40), there have been very few regulators of fungal effector expression
336 identified to date.

337 In this study, we developed a very simple forward-genetic screen to identify potential
338 regulators of effector gene expression in *M. oryzae*. Using a reporter line of *M. oryzae*, we selected
339 mutants showing constitutive expression of an effector-encoding gene, by simply picking mutants
340 with green fluorescent spores– a stage of development when effectors are not normally expressed.
341 Using whole-genome sequencing and bulked segregant analysis, we identified Rgs1, a well-known
342 regulator of G-protein signalling during appressorium development, as being necessary for
343 expression of the effector-encoding gene *MEP2*. Rgs1 is necessary for the repression of
344 transcription of a group of effector-encoding genes in conidia, that are among a group of 697 genes
345 which are Rgs1-dependent. This repression is clearly important biologically, as over-expressing
346 Rgs1 during plant infection leads to a reduction in pathogen fitness.

347 Rgs1 is one of a group of 8 RGS proteins in *M. oryzae* that play distinct and overlapping
348 regulatory functions (17). Rgs1 is involved in mediating perception of a hard, hydrophobic surface
349 to induce appressorium morphogenesis. The non-canonical G-protein coupled receptor (GPCR),
350 Pth11, responds to this inductive cue, leading to dissociation of the Gα-sub-unit, MagA, from the
351 heterotrimeric G$\alpha\beta\gamma$ complex (17). MagA activity is regulated by Rgs1, to control the levels of cAMP,
352 leading to activation of the cAMP/protein kinase A pathway (17, 31). In addition, Rgs1 negatively
353 regulates the Gα-sub-unit protein, MagB, during asexual conidiation (15) and mating (16). Rgs1 is
354 phosphorylated by casein kinase 2 at the plasma membrane and late endosome, which is essential
355 for its GTPase-activating protein (GAP) activity (17). RGS proteins are well known to mediate
356 GPCR signalling functions due to DEP-domain-mediated tethering (41), which is consistent with
357 the tandem DEP domains found in Rgs1 (31). An important question arising from this work is how
358 an RGS protein, such as Rgs1, could also exert a transcriptional regulator function. It is not clear,
359 for instance, whether this is a direct function of Rgs1 or whether the RGS protein regulates
360 expression of additional transcription regulators via a cell signalling function. Previously, it was
361 reported that Rgs1 undergoes endoproteolytic cleavage to produce the DEP-DEP protein N-Rgs1,
362 and the RGS catalytic protein C-Rgs1 (15). This mirrors the endoproteolytic cleavage of the Sst2
363 RGS protein in *Saccharomyces cerevisiae*, which has been proposed to serve a regulatory function
364 of its RGS catalytic activity (41, 42). Interestingly, we found evidence in RNA-seq data from a time-

365 course of rice infection of a potential exon skipping event that may occur in *M. oryzae*, suggesting
366 that N-Rgs1 is preferentially generated during the pre-penetration stage of development.
367 Furthermore, the DEP-DEP N-Rgs1 protein is able to complement the Δ*rgs1* mutant phenotype,
368 while the RGS C-Rgs1 cannot. Additionally, Rgs1-insensitive alleles of MagA, MagB and MagC, or
369 GTPase-inactive or constitutive alleles of MagA and MagB, showed no effect on the effector-
370 regulatory ability of Rgs1. When considered together, this is consistent with a model whereby the
371 effector regulatory function of Rgs1 resides in N-Rgs1 and is associated with the pre-penetration
372 stage, when Rgs1 regulates MagA and cAMP levels during appressorium morphogenesis (15, 17,
373 31). Interestingly, N-Rgs1 also shows activity in a yeast transactivation assay. However, the
374 absence of DNA-binding activity in N-Rgs1, suggests that if the protein does have a transcriptional
375 regulatory function then it must act in association with other proteins. There are examples of RGS
376 proteins exerting transcriptional functions (43). In humans, for example, RGS2, RGS10, and
377 RGS12, are nuclear proteins, while RGS4, RGS14 and RGS16 are nucleocytoplasmic shuttle
378 proteins (44, 45). Human RGS6 is, furthermore, subject to complex alternative splicing with 36
379 distinct splice variants present that either localise to the cytoplasm, nucleus or nucleolus of neurons
380 in the brain (46). RGS12, meanwhile, has been shown to have transcriptional activity, which resides
381 solely in an N-terminal domain which can act as a transcriptional repressor and also has cell cycle-
382 regulating activities, independent of its RGS domain (43). In our experiments Rgs1 appears to
383 localise to the cytoplasm predominantly with some punctate distribution also observed, although
384 N-Rgs1 has also been reported to show endomembrane/vesicular localisation (31). It is therefore
385 possible that Rgs1 interacts with the plasma membrane or endomembrane compartments via its
386 DEP domains and exerts a signalling function that ultimately activates a downstream transcription
387 factor (47). The RGS protein FlbA in *Aspergillus niger*, for example, involved in regulation of
388 sporulation regulates expression of many downstream functions via a set of transcription factors,
389 including rpnR which regulates protein secretion and stress responses (48), and Fum21 which
390 regulates production of the mycotoxin fumonisin (49). We are currently screening putative
391 interactors of N-Rgs1 to identify its potential mode of action in the regulation of effector function
392 and investigating whether a sub-population of N-Rgs1 might enter the nucleus.
393 In summary, we have demonstrated a successful way to identify a novel regulator of
394 effector gene expression. By using a simple forward genetic screen, it has proven possible to
395 identify a regulator that ensures the correct temporal expression profile of a large group of at least
396 60 effector genes, preventing their premature expression prior to plant infection. This genetic
397 approach has therefore revealed an unexpected link between the developmental biology of the pre-
398 penetration stage of *M. oryzae*, regulated by the RGS protein Rgs1, and events that occur after
399 host cell invasion, including the expression of fungal effectors that suppress plant immunity and
400 contribute to rice blast disease.
401

402 **Materials and Methods**

403

404 **Fungal and plant growth conditions**

405 Growth and maintenance of *M. oryzae* isolates, media composition, nucleic acid extraction, and
406 fungal transformation were all performed as previously described (50). Strains were collected from
407 stocks and inoculated to solid complete medium (CM) and incubated at 24°C with a 12 hour light-
408 dark cycle. For plant infection, conidial suspensions of *M. oryzae* at 5 x10^4 conidia mL^{-1} in 0.2%
409 gelatin were spray inoculated onto 21-day-old rice seedlings of CO39 using an artist's airbrush.
410 Rice blast symptoms were scored using disease lesion density 5 days post-inoculation, as
411 described previously (50). DNA amplification, cDNA synthesis, and qRT-PCR were carried out
412 using standard procedures with specific primers (*SI appendix*, Table S1). Further details regarding
413 *M. oryzae* mutant generation, UV mutagenesis, and bulked segregant analysis are provided in *SI*
414 *Materials and Methods*.

415 **Appressorium development assays and leaf sheath infection**

416 Appressorium assay of rice blast fungus was performed as previously described (33). Briefly,
417 conidial suspensions were prepared at 5 x10^4 conidia mL^{-1} in water, and 20 µL of the suspension
418 placed onto the surface of a hydrophobic coverslip (Corning) and incubated in a controlled
419 environment chamber at 24°C. Live cell imaging of plant penetration, effector localization in
420 invasive hyphae and growth of the fungus *in planta* used a leaf sheath assay, described previously .
421 Briefly, a suspension of 5 x10^4 conidia mL^{-1} was prepared in 0.2% gelatin and inoculated into the
422 hollow space of the leaf sheath tissue that was dissected from the flag leaf of 21-day-old rice
423 seedlings of cultivar CO-39. A single epidermal layer of the leaf sheath was trimmed and mounted
424 for microscopy (23).

425 **Live Cell Imaging and Quantitative Analysis**

426 To screen the mutant, Sterile water was used to harvest spores from a 7-day old *M. oryzae* CM
427 plate culture, before filtering through sterile Miracloth (Calbiochem). A 20 µL aliquot of suspension
428 was transferred to a microscope slide and covered with a clean cover slip before imaging with
429 epifluorescence and differential interference contrast (DIC) microscopy. For epifluorescence and
430 differential interference contrast (DIC) microscopy, samples were observed using an IX-81 inverted
431 microscope (Olympus) and a UPlanSApox100/1.40 oil objective. Images were captured using a
432 photometrics CoolSNAP HQ2 camera system incorporated with MetaMorph software packages
433 (MDS Analytical Technologies, Winersh, UK). Epifluorescence parameters for GFP were excitation
434 488 at nm, and RFP excitation at 561nm. Quantification of fluorescence intensity was performed
435 using Fuji-ImageJ (51). To measure fluorescence intensity, conidia of interest were selected using
436 drawing tools. "Measure" was used to obtain the "Integrated Density" (ID) for the conidial

437 fluorescence signal. The background region next to the conidium of interest was selected and
438 measured to obtain the pixel value for "mean fluorescence of background readings" (MFBR). The
439 values of conidia and background were extracted and saved to calculate the corrected cell
440 fluorescence (CCF) using the formula: CCF = Integrated Density (ID) - mean fluorescence of
441 background readings (MFBR). Details of RNA extraction, RNA-seq analysis, quantitative real-time
442 PCR, yeast transactivation assay, and one-yeast hybrid system are given in *SI Materials and*
443 *Methods*.

444 **SI Materials and Methods**
445
446 **Generation of *M. oryzae* mutants and strains expressing GFP or RFP fusions**

447 To generate *M. oryzae* transformants expressing Mep2-GFP, the full-length coding sequence of
448 *MEP2* (25) was cloned with 1.5 kb of upstream promoter sequence and fused at its C-terminus to
449 eGFP. The Mep2-GFP plasmid was constructed using the linearized pCB1532 carrying the
450 acetolactate synthase gene which confers resistance to sulfonylurea. Independent *M. oryzae*
451 transformants were used for screening and selected on medium with sulfonylurea (400 µg mL^{-1}) for
452 fluorescence localization and quantification. In-Fusion cloning (Clontech Laboratories) was used to
453 generate $RGS1^{WT}$, $rgs1^{cer7}$, N-Rgs1, C-Rgs1, Bas113-RFP, Rgs1-GFP, Bas3-RFP, $MagA^{G187S}$,
454 $MagB^{G183S}$, $MagA^{Q208L}$, $MagB^{Q204L}$, $MagC^{G184S}$, $MagB^{G42R}$. $MagA^{G187S}$, $MagB^{G183S}$, and $MagC^{G184S}$,
455 and *pToxA-Rgs1-GFP* strains, using primers in Table S1. $RGS1^{WT}$, $rgs1^{cer7}$, N-Rgs1, C-Rgs1, were
456 cloned under control of the *RGS1* native promoter (1 kb) and native terminator (600bp) sequence,
457 except N-Rgs1 which was fused to the TrpC terminator., Bas113-RFP, Rgs1-GFP, Bas3-RFP, and
458 pToxA-Rgs1-GFP were cloned with their full protein coding sequences without stop codons driven
459 by their native promoters, except *pToxA-Rgs1-GFP* which was fused with ToxA promoter at its N-
460 terminus. The fragments were then fused with eGFP in-frame at the C-terminus. $MagA^{G187S}$,
461 $MagB^{G183S}$, $MagA^{Q208L}$, $MagB^{Q204L}$, $MagC^{G184S}$, $MagB^{G42R}$. $MagA^{G187S}$, $MagB^{G183S}$, and $MagC^{G184S}$
462 were cloned with their native promoters and point mutations generated as described previously
463 (15). Constructs were routinely cloned into a SpeI and NotI digested StrataClone vector, pSC-A-
464 amp/kan, with the BAR gene conferring bialophos resistance (52, 53). Plasmids were then
465 introduced into *M. oryzae* by fungal transformation (54) and transformants selected by growing on
466 CM supplemented with glufosinate (30 µg mL^{-1}). All transformants were evaluated by PCR using
467 primers flanking the predicted insertion to select those carrying single plasmid insertions. This was
468 subsequently verified by whole genome sequencing.

469 Targeted gene replacement of the Rgs1-encoding gene and native allelic replacement of *RGS1*
470 with the hygromycin phosphotransferase gene cassette (HYG), bestowing hygromycin B resistance,
471 were performed using the split-marker strategy as previously described with minor modifications
472 (55-57). Briefly, we first amplified the 1 kb *HY* and 0.7 kb length YG fragments using the primers

473 M13F and HY split for *HY*, M13R and YG split for *YG* (55). To create the fusion in the first round of
474 PCR, a 3.2 kb length fragment of DNA sequence of the mutant allele of *RGS1*^{cer7} carrying the
475 identified SNP, including 600 bp downstream sequence (3'-UTR), was amplified using allele-
476 specific primers (P1 and P2). The 5' end of primer P1 is 97 bp upstream of the SNP. The 5' end of
477 primer P2 included an extension overhanging sequence complementary to the M13F primer site.
478 A 1.4 kb of DNA fragment was amplified from the right flank of the *RGS1* gene from *cer7* using
479 allele-specific primers (P3 and P4). An overhanging sequence was added to the 5' end of primer
480 P3, complementary to the M13R sequence. The 5' end of the right flank is 100 bp downstream of
481 the 3'-UTR. Isolated genomic DNA of the *cer7* strain was used as template for the PCR. After
482 amplification the two initial PCR products were mixed with *HY* and *YG*, respectively, and used as
483 templates for a second round of PCR. During the second round PCR, primers P1 and *HY* split were
484 used to amplify a 4.2 kb length fragment, and primers P4 and *YG* split were used to amplify a 2.1
485 kb length fragment. These products were gel-purified, mixed in equimolar concentrations and
486 transformed into the *Mep2-GFP* strain of *M.oryzae*. The fragments were used to replace the original
487 wild type *RGS1* allele, based on three crossover events (7). The joined *HYG* allele confers
488 hygromycin B resistance and allowed transformants to grow on CM plates supplemented with
489 hygromycin B. We obtained 25 hygromycin B resistant transformants, isolated genomic DNA from
490 these and performed PCR to amplify the fragment from 5' of left flank of *RGS1* gene locus to 3' of
491 right flank, using primers P1 and P4. Targeted allelic replacement transformants had an additional
492 1.5 kb sequence, generating an 8.0kb amplicon, while unsuccessful transformants still contained
493 the wild type *RGS1* allele on a 6.5 kb amplicon. Transformants were selected on complete medium
494 (CM) (1) supplemented with hygromycin B (200 µg mL^{-1}) and assessed by PCR to amplify the
495 specific allele which was then sequenced to ensure the *cer7* SNP was present. All mutants and
496 transformants generated in this study are listed in Table S2.

497 **UV mutagenesis of *M. oryzae***

498 Conidia of *M. oryzae* were harvested from a CM plate culture using a sterile plastic spreader with
499 2 mL sterile water. Conidial suspensions were generated in 200 µL sterile distilled water containing
500 0.1% Tween 20, at a concentration of 5 x10^{5} conidia mL^{-1} before spreading onto the surface of
501 modified CM agar containing 1% sorbose. The Petri dish was exposed without its lid under UV light
502 at 254 nm using a UV crosslinker (Stratagene) in the dark. A calibration test was first performed to
503 estimate the time necessary to result in either a 40% or 90% kill rate. After UV mutagenesis, plates
504 were immediately wrapped in aluminium foil to avoid DNA photo-repair after ultraviolet light-
505 induced DNA damage. Plates were then incubated at 26°. After 2-3 days, the foil was removed and
506 the plates were grown for a further 4-5 days. Putative mutants were selected based on expression
507 of Mep2-GFP using an epifluorescence stereo microscope Leica M205 FCA. The candidate
508 mutants were then collected using a sterile needle onto fresh CM agar and incubated for 5 days.

509 To perform single spore isolation for each potential candidate mutant, a conidial suspension from
510 each plate was sprayed onto 4% water agar and four single conidia were individually removed
511 using a sterile mounted needle. The resulting single conidia were transferred onto 48 well plates
512 containing CM. The purified mutant strains were then screened for expression of Mep2-GFP as
513 described above and stored as filter paper stocks at -20°C.

514 **Bulked segregant analysis, SNP calling and alternative splicing analysis**

515 Bulked segregant analysis (BSA) was performed, as previously described with minor modifications
516 (58). Briefly, the *cer7* mutant strain (*Mat1-1*) and wild-type strain TH3 (*Mat1-2*) were grown at 24°C
517 for 7 days on oatmeal agar medium, and then at 18°C until flask-shaped perithecia were visible.
518 After 4-6 weeks growth, mature perithecia were removed and transferred onto 4% water agar
519 medium. The collected perithecia were crushed with a sterile needle to release asci. Mature asci
520 were removed and ascospores dissected under a Leica M205 FCA stereo microscope using a
521 micro-manipulator (Singer Instruments). Collected ascospores were transferred individually to a
522 48-well plate containing CM and incubated for 5 days (59). Progeny were next screened by
523 phenotypic assessment of fluorescence. Genomic DNA was then extracted from ascospore
524 progeny, as described previously (54). Equal amounts of DNA from each progeny (100ng per
525 progeny) were then bulked. DNA samples were bulked into two samples: wild-type progeny
526 showing low expression of Mep2-GFP, and mutant progeny showing highly expressed Mep2-GFP.
527 The two samples were sequenced using an Illumina HiSeq 2500 generating 125-bp paired-end
528 sequences (University of Exeter Sequencing Service). Low-quality reads were filtered using
529 Trimmomatic (60). SNP calling analysis was performed, as described previously with minor
530 modifications (58). Filtered reads were mapped to the *M. oryzae* 70-15 reference genome
531 (fungi.ensembl.org/Magnaporthe_oryzae/) using Bowtie2 with default parameters (61). Varscan
532 (62) was then used to discover variants by inputting BAM files generated from alignment of reads
533 of the genome sequence of the *cer7* mutant, pooled BSA samples, and the parental Mep2-GFP
534 strain of Guy11 used for mutagenesis. To discover SNPs, filtering was applied based on a minimum
535 read depth of 50 and minimum base identity of 95%. The Integrative Genome Viewer (IGV) (63)
536 was used to manually inspect variants from read alignment for evidence of mutations by input of
537 corresponding bam files.

538 For alternative splicing analysis, BAM files were generated using RSubread (v.2.10.5) with
539 default settings (64). Putative alternative splicing events of *RGS1* were analyzed based on
540 transcript read densities and visualized using IGV software (63). Peptide sequences of all coding
541 genes in version 8.0 of *M. oryzae* genome sequence were used to predict effectors by EffectorP-
542 2.0 as described (25). Verification of the insertion site of *MEP2-GFP* at a single site was verified by
543 whole genome assembly. Raw reads were aligned to the full plasmid sequence of pCB1532 using
544 Bowtie2 v2.2.9. The sorted BAM file was loaded into the IGV genome viewer to visualize the

545 coverage of raw reads across the Mep2-GFP sequence. The resulting reads aligned to the plasmid
546 and flanking region of the plasmid insertion site were extracted. The total raw reads were realigned
547 against the extracted reads using Exonerate v2.2.0 (32), showing at least 50 bp alignment without
548 any gap, representing reads located at the junction between the inserted plasmid and *M. oryzae*
549 genome. The resulting reads were then aligned against *M. oryzae* genome using Exonerate v2.2.0
550 and the location of insertion of plasmid visualized via IGV to confirm that the reads aligned to a
551 single locus in Chr1 as a single copy insertion.

552 **RNA extraction, RNA-seq analysis and quantitative real-time PCR**

553 Conidia from *cer7*, *Δrgs1*, and Guy11 were harvested from 7-day old CM agar plates. Total RNA
554 was extracted from conidia using the Qiagen RNeasy Plant Mini kit according to the manufacturer's
555 instructions. RNA-seq libraries were prepared using 10 μg of total RNA for Illumina HiSeq 2500
556 generating 150-bp paired-end sequences (Novogene, Beijing). Low quality reads were filtered by
557 Trimmomatic v0.32 prior to the alignment against version 8.0 of *M. oryzae* genome sequence using
558 bowtie2 (version 2.3.4.3). Quality of alignment was assessed by qualimap2 (version 2.2.1).
559 Pearson correlation and principal component analysis was performed to determine correlation
560 between the samples. The sva package was used to remove batch effects (65). Differentially
561 expressed genes were determined by DESeq2 through a threshold of log2FC and adjusted p-
562 values ($p<0.05$). for enrichment analysis, Clusterprofiler was used to performed KEGG metabolic
563 pathway enrichment analysis (66). For qRT-PCR, an Affinity Script QPCR cDNA Synthesis Kit was
564 used to generate cDNA, according to manufacturer's instructions. Briefly, a reaction premixed with
565 10 μL First-Strand Master Mix, 3μL of oligo(dT) primer, 1 μL of AffinityScript RNase Block enzyme
566 mixture, and 3 μg total RNA, was prepared and incubated at 25 °C for 5 min. The sample was
567 incubated at 42 °C for 15 min to allow cDNA synthesis, before further incubation at 95 °C for 5 min
568 to terminate the cDNA synthesis reaction. Quantitative real-time PCR (qPCR) analysis was
569 conducted using the Stratagene Mx3000TM Real-Time PCR. Each reaction contained 1.25 μL of
570 606 a 1:5 (v/v) dilution of cDNA, 0.2 μM of each primer and 1X SYBR® Premix Ex Taq™ (Tli RNase
571 H plus, RR420A, Takara) in a total reaction volume of 12.5 μL. PCR conditions were: 1 cycle of 1
572 min at 95°C; 40 cycles of 5 s at 95°C and 20 s at 60°C; and a final cycle of 1 min at 95°C, 30 s at
573 58°C and 30 s at 95°C for the dissociation curve. For measurement of the fold change, an efficiency
574 corrected calculation model was made using the formula ((target) ΔCt target (control – sample)) /
575 (housekeeping) ΔCt housekeeping (control – sample) (67).

576 **Western blot analysis**

577 To test *RGS1* levels in vegetative and invasive growth, total protein was extracted from mycelium
578 and infected rice leaf sheath using *M. oryzae* strains *ToxAp:GFP* (Control) and *RGS1p:GFP-RGS1*.
579 For vegetative growth, mycelium was prepared from CM shake cultures (125 rpm) at 24°C for 48
580 h. Mycelium was then filtered, washed in distilled water and frozen in liquid nitrogen. For invasive

581 growth, leaf sheath inoculation assays were performed, as previously reported (68) and frozen in
582 liquid nitrogen after 32 hpi. Frozen samples were ground to fine powder in liquid nitrogen using a
583 pestle and mortar. The powder was mixed with 2 times weight/volume ice-cold extraction buffer
584 (10% glycerol, 25 mM Tris pH 7.5, 1 mM EDTA, 150 mM NaCl, 2% w/v PVPP, 10 mM DTT, 1×
585 protease inhibitor cocktail (Sigma), 0.1% Tween 20 (Sigma)), centrifuged at 10,000g at 4°C for 10–
586 20 min, and the supernatant passed through a 0.45 µm Minisart® syringe filter. Proteins were
587 separated by SDS-PAGE and transferred onto a polyvinylidene difluoride (PVDF) membrane using
588 a Trans-Blot turbo transfer system (Bio-Rad). PVDF membrane was blocked with 2% bovine serum
589 albumin (BSA) in Tris-buffered saline and 1% Tween 20 (Sigma). GFP detection was carried using
590 a GFP (B2):sc-9996 horseradish peroxidase (HRP)-conjugated antibody (Santa Cruz
591 Biotechnology, Santa Cruz, CA). An anti-actin antibody was used as the loading control for fungal
592 and plant protein. Pierce ECL Western Blotting Substrate (Thermo Fisher Scientific) was used for
593 detection. Membranes were imaged using ImageQuant LAS 4000 luminescent imager (GE Life
594 Sciences).

595 **Yeast Transactivation Assay and Yeast One-Hybrid Analysis**

596 The transcriptional activity and DNA-binding ability of N-Rgs1 and Rgs1 were tested in
597 *Saccharomyces cerevisiae* strain Y2HGold. Sequences encoding N-Rgs1 and C-Rgs1 were
598 amplified from cDNA derived from total RNA of Guy11 conidia. Fragments were cloned into
599 pGBKT7 (BD) and pGADT7 (AD) vectors, respectively, by in-fusion cloning (In-Fusion Cloning kit;
600 Clontech Laboratories). pGBKT7(BD)-N-Rgs1, pGBKT7(BD)-Rgs1 were used to test
601 transactivation activity, and pGADT7(AD)- N-Rgs1, pGADT7(AD)-Rgs1 were used to test DNA-
602 binding ability. The empty vectors were co-transformed and used to test the transcriptional
603 activation as a negative control. The vectors pGBKT7-53 and pGADT7-T were used as the positive
604 control. Empty un-linearized bait vector pGBKT7 and prey vector pGADT7 were used as negative
605 controls. BKT variants and GAD variants were co-transformed into chemically competent Y2HGold
606 yeast cell following the manufacturer's manual. Successfully transformed yeast colonies were
607 inoculated in 2mL of liquid SD/-Leu/-Trp selection media for overnight growth at 30°C. The yeast
608 samples were then used to produce dilutions of OD_{600} 1, 1^{-1}, 1^{-2}, 1^{-3}, and 1^{-4}, respectively. Cell
609 suspensions in 10µL droplets of each dilution were spotted on a SD/-Leu/-Trp/-His to determine
610 the transactivation activity and DNA-binding ability, after 72 h growth at 30°C.

611 For yeast one-hybrid experiments, the Matchmaker Gold Yeast One-hybrid System kit (Takara Bio,
612 USA) was used according to manufacturer's instructions. Briefly, a 1 kb fragment upstream of the
613 *MEP2* gene was prepared as the bait sequence and ligated into digested vector pAbAi, which
614 carries the bAr gene (AUR-1C) that confers resistance to AbA (Aureobasidin A) (Takara Bio, USA).
615 The p-AbAi-*MEP2* vector, and positive control vector p53-AbAi were digested with BbsI, and then
616 transformed into yeast strain Y1HGold (69), respectively. Y1HGold [*MEP2p* / AbAi] and Y1HGold

[p53 / AbAi] was screened by growing on SD/-Ura. The minimum inhibitory concentration of AbA (200 ng/mL) for the bait strain was determined by growing on SD/-Ura/AbA medium. The cDNA sequence encoding N-Rgs1 was amplified from total RNA by RT-PCR using primers with overhanging sequences the prey vector pGADT7. The plasmid pGADT7- was then transformed into bait yeast strain Y1HGold [*MEP2p*/AbAi], and Y1HGold[p53/AbAi], respectively. The yeast samples were used to produce dilutions of OD600 1, 1^{-1}, 1^{-2}, 1^{-3}, and 1^{-4}, respectively. SD/-Leu/AbA^{200} medium was used to test the *MEP2p*/N-Rgs1 interaction.

Acknowledgments

This project was supported by a European Research Council Advanced Investigator award (to NJT) under the European Union's Seventh Framework Programme FP7/2007-2013/ERC Grant Agreement 294702 GENBLAST, a grant to NJT from The Gatsby Charitable Foundation, and a Halpin Scholarship to BT.

Author Contributions

Author contributions: B.T. and N.J.T. designed research; B.T., X.Y., A.J.F., C.M., and N.C.M. performed experiments. B.T., and D.M.S. performed analysis of data. B.T., L.S.R., and N.J.T. wrote the paper.

The authors declare no conflict of interest.

Data deposition: RNA-seq data of *M. oryzae* and the genome sequence of *cer7* mutant strain reported in this paper were deposited in the European Nucleotide Archive - EMBL-EBI database under accession number: PRJEB45710.

SI References

1. L. Lo Presti *et al.*, Fungal effectors and plant susceptibility. *Annual review of plant biology* **66**, 513-545 (2015).
2. S. Kamoun, A catalogue of the effector secretome of plant pathogenic oomycetes. *Annu. Rev. Phytopathol.* **44**, 41-60 (2006).
3. P. Skamnioti, S. J. Gurr, Against the grain: safeguarding rice from rice blast disease. *Trends Biotechnol* **27**, 141-150 (2009).
4. T. Y. Toruño, I. Stergiopoulos, G. Coaker, Plant-pathogen effectors: cellular probes interfering with plant defenses in spatial and temporal manners. *Annual review of phytopathology* **54**, 419 (2016).
5. J. Jeon *et al.*, Transcriptome Profiling of the Rice Blast Fungus Magnaporthe oryzae and Its Host Oryza sativa During Infection. *Molecular Plant-Microbe Interactions®* **33**, 141-144 (2019).
6. S. Tanaka *et al.*, Neofunctionalization of the secreted Tin2 effector in the fungal pathogen Ustilago maydis. *Nature Microbiology* **4**, 251-257 (2019).
7. L. Meile *et al.*, Chromatin Dynamics Contribute to the Spatiotemporal Expression Pattern of Virulence Genes in a Fungal Plant Pathogen. *mBio* **11**, e02343-02320 (2020).
8. G. Mosquera, M. C. Giraldo, C. H. Khang, S. Coughlan, B. Valent, Interaction Transcriptome Analysis Identifies Magnaporthe oryzae BAS1-4 as Biotrophy-Associated Secreted Proteins in Rice Blast Disease. *The Plant Cell* **21**, 1273 (2009).
9. J. Fernandez, K. Orth, Rise of a cereal killer: the biology of Magnaporthe oryzae biotrophic growth. *Trends in microbiology* **26**, 582-597 (2018).

10. A. B. Eseola *et al.*, Investigating the cell and developmental biology of plant infection by the rice blast fungus Magnaporthe oryzae. *Fungal Genetics and Biology* **154**, 103562 (2021).
11. L. S. Ryder *et al.*, The appressorium at a glance. *Journal of Cell Science* **135**, jcs259857 (2022).
12. J. R. Xu, J. E. Hamer, MAP kinase and cAMP signaling regulate infection structure formation and pathogenic growth in the rice blast fungus Magnaporthe grisea. *Genes Dev* **10**, 2696-2706 (1996).
13. R. A. Wilson, N. J. Talbot, Under pressure: investigating the biology of plant infection by Magnaporthe oryzae. *Nat Rev Microbiol* **7**, 185-195 (2009).
14. K. Adachi, J. E. Hamer, Divergent cAMP signaling pathways regulate growth and pathogenesis in the rice blast fungus Magnaporthe grisea. *The Plant cell* **10**, 1361-1374 (1998).
15. H. Liu *et al.*, Rgs1 regulates multiple Galpha subunits in Magnaporthe pathogenesis, asexual growth and thigmotropism. *The EMBO journal* **26**, 690-700 (2007).
16. H. Zhang *et al.*, Eight RGS and RGS-like Proteins Orchestrate Growth, Differentiation, and Pathogenicity of Magnaporthe oryzae. *PLOS Pathogens* **7**, e1002450 (2011).
17. R. Yu *et al.*, The rice blast fungus MoRgs1 functioning in cAMP signaling and pathogenicity is regulated by casein kinase MoCk2 phosphorylation and modulated by membrane protein MoEmc2. *PLoS pathogens* **17**, e1009657 (2021).
18. M. Yi, B. Valent, Communication Between Filamentous Pathogens and Plants at the Biotrophic Interface. *Annual Review of Phytopathology* **51**, 587-611 (2013).
19. M. C. Giraldo *et al.*, Two distinct secretion systems facilitate tissue invasion by the rice blast fungus Magnaporthe oryzae. *Nat Commun* **4**, 1996 (2013).
20. C. H. Khang *et al.*, Translocation of Magnaporthe oryzae Effectors into Rice Cells and Their Subsequent Cell-to-Cell Movement. *The Plant Cell* **22**, 1388 (2010).
21. S. Zhang, J.-R. Xu, Effectors and effector delivery in Magnaporthe oryzae. *PLoS pathogens* **10**, e1003826-e1003826 (2014).
22. T. A. Mentlak *et al.*, Effector-mediated suppression of chitin-triggered immunity by Magnaporthe oryzae is necessary for rice blast disease. *The Plant Cell* **24**, 322-335 (2012).
23. W. Sakulkoo *et al.*, A single fungal MAP kinase controls plant cell-to-cell invasion by the rice blast fungus. *Science* **359**, 1399-1403 (2018).
24. K. de Guillen *et al.*, Structure analysis uncovers a highly diverse but structurally conserved effector family in phytopathogenic fungi. *PLoS pathogens* **11**, e1005228 (2015).
25. X. Yan *et al.*, The transcriptional landscape of plant infection by the rice blast fungus Magnaporthe oryzae reveals distinct families of temporally co-regulated and structurally conserved effectors. *bioRxiv* (2022).
26. M. Tollot *et al.*, The WOPR protein Ros1 is a master regulator of sporogenesis and late effector gene expression in the maize pathogen Ustilago maydis. *PLoS pathogens* **12**, e1005697 (2016).
27. D. A. Jones *et al.*, A specific fungal transcription factor controls effector gene expression and orchestrates the establishment of the necrotrophic pathogen lifestyle on wheat. *Scientific reports* **9**, 1-13 (2019).
28. W. Zhang, J. Huang, D. E. Cook, Histone modification dynamics at H3K27 are associated with altered transcription of in planta induced genes in Magnaporthe oryzae. *PLoS genetics* **17**, e1009376 (2021).
29. R. A. Dean *et al.*, The genome sequence of the rice blast fungus Magnaporthe grisea. *Nature* **434**, 980-986 (2005).
30. R. W. Michelmore, I. Paran, R. Kesseli, Identification of markers linked to disease-resistance genes by bulked segregant analysis: a rapid method to detect markers in specific genomic regions by using segregating populations. *Proceedings of the national academy of sciences* **88**, 9828-9832 (1991).

31. R. Ramanujam, X. Yishi, H. Liu, N. I. Naqvi, Structure-function analysis of Rgs1 in Magnaporthe oryzae: role of DEP domains in subcellular targeting. *PLoS One* **7**, e41084-e41084 (2012).
32. G. S. C. Slater, E. Birney, Automated generation of heuristics for biological sequence comparison. *BMC bioinformatics* **6**, 1-11 (2005).
33. M. Osés-Ruiz *et al.*, Appressorium-mediated plant infection by Magnaporthe oryzae is regulated by a Pmk1-dependent hierarchical transcriptional network. *Nature microbiology* **6**, 1383-1397 (2021).
34. Y.-L. Fang, Y.-L. Peng, J. Fan, The Nep1-like protein family of Magnaporthe oryzae is dispensable for the infection of rice plants. *Scientific reports* **7**, 1-10 (2017).
35. M.-H. Chi, S.-Y. Park, S. Kim, Y.-H. Lee, A novel pathogenicity gene is required in the rice blast fungus to suppress the basal defenses of the host. *PLoS pathogens* **5**, e1000401-e1000401 (2009).
36. M. Hasegawa *et al.*, Phytoalexin Accumulation in the Interaction Between Rice and the Blast Fungus. *Molecular Plant-Microbe Interactions®* **23**, 1000-1011 (2010).
37. D. Lanver *et al.*, The biotrophic development of Ustilago maydis studied by RNA-seq analysis. *The Plant Cell* **30**, 300-323 (2018).
38. M. Franceschetti *et al.*, Effectors of filamentous plant pathogens: commonalities amid diversity. *Microbiology and Molecular Biology Reviews* **81**, e00066-00016 (2017).
39. K. Seong, K. Krasileva, Comparative computational structural genomics highlights divergent evolution of fungal effectors. *bioRxiv* (2022).
40. X. Tang, Y. Xiao, J.-M. Zhou, Regulation of the type III secretion system in phytopathogenic bacteria. *Molecular plant-microbe interactions* **19**, 1159-1166 (2006).
41. D. R. Ballon *et al.*, DEP-domain-mediated regulation of GPCR signaling responses. *Cell* **126**, 1079-1093 (2006).
42. G. A. Hoffman, T. R. Garrison, H. G. Dohlman, Endoproteolytic processing of Sst2, a multidomain regulator of G protein signaling in yeast. *Journal of Biological Chemistry* **275**, 37533-37541 (2000).
43. T. K. Chatterjee, R. A. Fisher, RGS12TS-S localizes at nuclear matrix-associated subnuclear structures and represses transcription: structural requirements for subnuclear targeting and transcriptional repression. *Molecular and cellular biology* **22**, 4334-4345 (2002).
44. T. K. Chatterjee, R. A. Fisher, Cytoplasmic, nuclear, and golgi localization of RGS proteins: evidence for N-terminal and RGS domain sequences as intracellular targeting motifs. *Journal of Biological Chemistry* **275**, 24013-24021 (2000).
45. N. H. Harbin, S. N. Bramlett, C. Montanez-Miranda, G. Terzioglu, J. R. Hepler, RGS14 regulation of post-synaptic signaling and spine plasticity in brain. *International Journal of Molecular Sciences* **22**, 6823 (2021).
46. T. K. Chatterjee, Z. Liu, R. A. Fisher, Human RGS6 gene structure, complex alternative splicing, and role of N terminus and G protein gamma-subunit-like (GGL) domain in subcellular localization of RGS6 splice variants. *J Biol Chem* **278**, 30261-30271 (2003).
47. S. V. Consonni, M. M. Maurice, J. L. Bos, DEP domains: structurally similar but functionally different. *Nature Reviews Molecular Cell Biology* **15**, 357-362 (2014).
48. D. Aerts *et al.*, FlbA-regulated gene rpnR is involved in stress resistance and impacts protein secretion when Aspergillus niger is grown on xylose. *Applied and environmental microbiology* **85**, e02282-02218 (2019).
49. D. Aerts *et al.*, The FlbA-regulated predicted transcription factor Fum21 of Aspergillus niger is involved in fumonisin production. *Antonie Van Leeuwenhoek* **111**, 311-322 (2018).
50. N. J. Talbot, D. J. Ebbole, J. E. Hamer, Identification and characterization of MPG1, a gene involved in pathogenicity from the rice blast fungus Magnaporthe grisea. *The Plant Cell* **5**, 1575 (1993).
51. J. Schindelin *et al.*, Fiji: an open-source platform for biological-image analysis. *Nature methods* **9**, 676-682 (2012).

52. R. J. Lindsay, M. J. Kershaw, B. J. Pawlowska, N. J. Talbot, I. Gudelj, Harbouring public good mutants within a pathogen population can increase both fitness and virulence. *eLife* **5**, e18678 (2016).
53. L. S. Ryder *et al.*, A sensor kinase controls turgor-driven plant infection by the rice blast fungus. *Nature* **574**, 423-427 (2019).
54. N. J. Talbot, D. J. Ebbole, J. E. Hamer, Identification and characterization of MPG1, a gene involved in pathogenicity from the rice blast fungus Magnaporthe grisea. *The Plant Cell* **5**, 1575-1590 (1993).
55. M. J. Kershaw, N. J. Talbot, Genome-wide functional analysis reveals that infection-associated fungal autophagy is necessary for rice blast disease. *Proceedings of the National Academy of Sciences* **106**, 15967 (2009).
56. W. Sakulkoo *et al.*, A single fungal MAP kinase controls plant cell-to-cell invasion by the rice blast fungus. *Science* **359**, 1399 (2018).
57. N. L. Catlett, B.-N. Lee, O. Yoder, B. G. Turgeon, Split-marker recombination for efficient targeted deletion of fungal genes. *Fungal Genetics Newsletter*, 9-11 (2003).
58. M. J. Kershaw *et al.*, Conidial morphogenesis and septin-mediated plant infection require Smo1, a Ras GTPase-activating protein in Magnaporthe oryzae. *Genetics* **211**, 151-167 (2019).
59. N. J. Talbot *et al.*, MPG1 encodes a fungal hydrophobin involved in surface interactions during infection-related development of Magnaporthe grisea. *The Plant Cell* **8**, 985-999 (1996).
60. A. M. Bolger, M. Lohse, B. Usadel, Trimmomatic: a flexible trimmer for Illumina sequence data. *Bioinformatics* **30**, 2114-2120 (2014).
61. B. Langmead, S. L. Salzberg, Fast gapped-read alignment with Bowtie 2. *Nat Methods* **9**, 357-359 (2012).
62. D. C. Koboldt *et al.*, VarScan 2: somatic mutation and copy number alteration discovery in cancer by exome sequencing. *Genome Res* **22**, 568-576 (2012).
63. J. T. Robinson *et al.*, Integrative genomics viewer. *Nature biotechnology* **29**, 24-26 (2011).
64. Y. Liao, G. K. Smyth, W. Shi, The R package Rsubread is easier, faster, cheaper and better for alignment and quantification of RNA sequencing reads. *Nucleic acids research* **47**, e47-e47 (2019).
65. J. T. Leek, W. E. Johnson, H. S. Parker, A. E. Jaffe, J. D. Storey, The sva package for removing batch effects and other unwanted variation in high-throughput experiments. *Bioinformatics* **28**, 882-883 (2012).
66. G. Yu, L.-G. Wang, Y. Han, Q.-Y. He, clusterProfiler: an R package for comparing biological themes among gene clusters. *OMICS* **16**, 284-287 (2012).
67. K. J. Livak, T. D. Schmittgen, Analysis of Relative Gene Expression Data Using Real-Time Quantitative PCR and the 2−ΔΔCT Method. *Methods* **25**, 402-408 (2001).
68. P. Kankanala, K. Czymmek, B. Valent, Roles for rice membrane dynamics and plasmodesmata during biotrophic invasion by the blast fungus. *The Plant Cell* **19**, 706-724 (2007).
69. J. N. Abelson, M. I. Simon, C. Guthrie, G. R. Fink, *Guide to yeast genetics and molecular biology* (Gulf Professional Publishing, 2004).

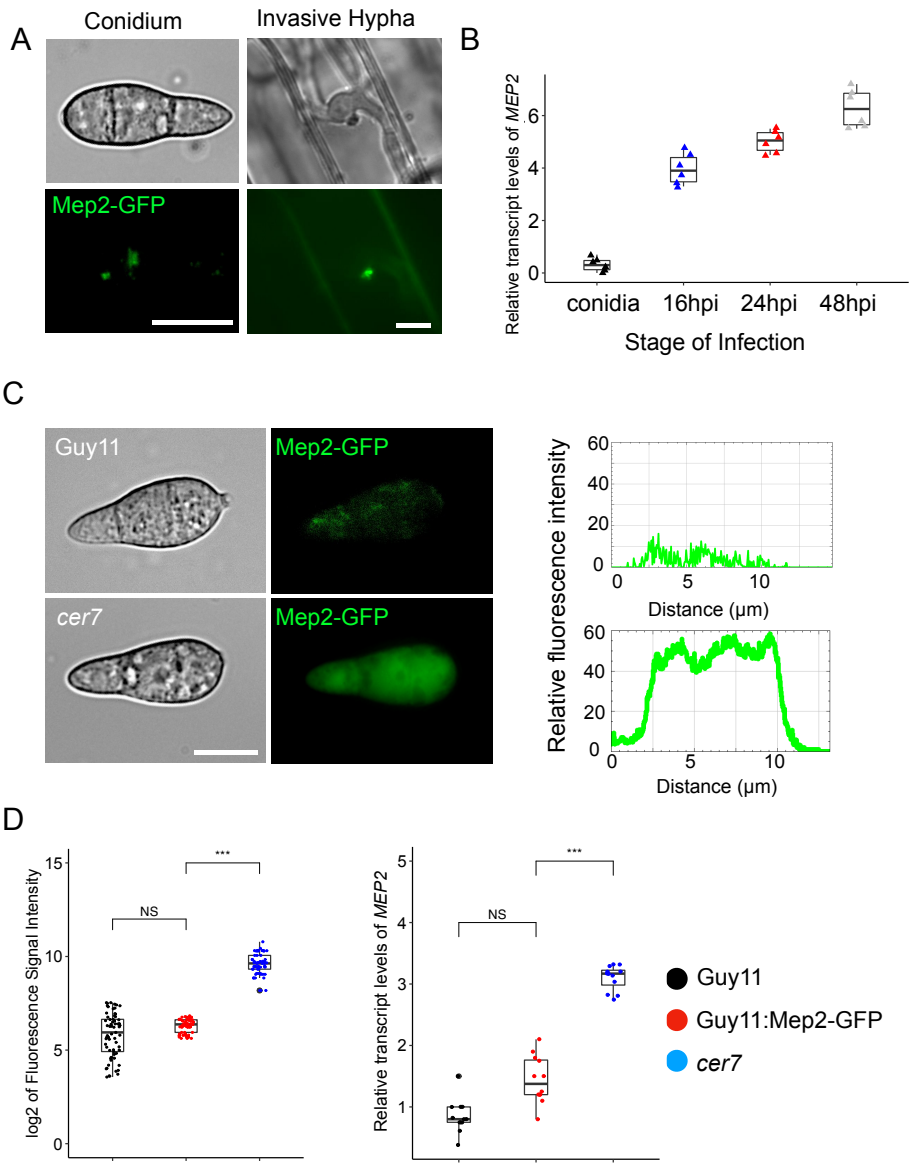

Figure 1. A forward genetic screen identified the *cer7* mutant of *M. oryzae* (***A***) Micrographs showing differential expression of Mep2-GFP at the BIC in invasive hyphae and basal expression in conidia of the wild type *M. oryzae strain* Guy11. (Scale bar, 10 µm). BIC localization was imaged in rice leaf sheath tissue inoculated with conidia of Guy11:Mep2-GFP at 32 hpi. (***B***) Boxplots to show relative transcripts of *MEP2* as log2 fold changes values in invasive hyphae of Guy11. The samples were harvested from Guy11 conidia and leaf sheath harvested at 16hpi, 24hpi, and 48hpi. n=6 experiments. Expression is shown relative to the *M. oryzae* actin gene. (***C***) Micrographs and line-scan graphs showing the constitutive fluorescence signal of Mep2-GFP in mutant strain *cer7* conidia, compared to the wild-type Guy11 (Scale bar, 10 µm). (***D***) Box plots to show fluorescence intensities of Mep2-GFP as log2 values and relative abundance of *MEP2* transcripts as log2 fold change values in qRT-PCR. Colours correspond to Guy11 (black), *cer7* (red), and Guy11:*MEP2-GFP* (blue). Significance between groups of samples was performed using Unpaired Student's t-test. ***p<0.001, *p<0.05, NS = no significant difference.

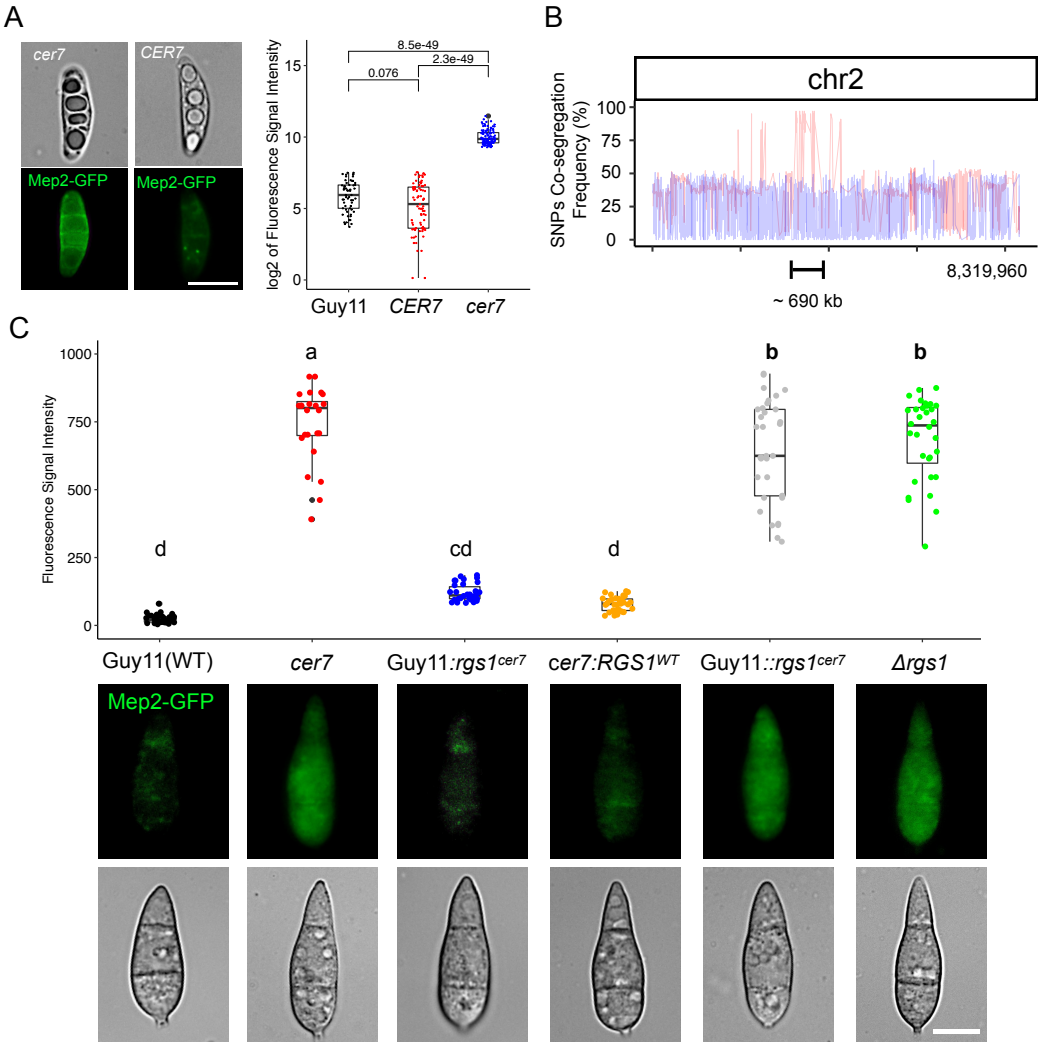

Figure 2. Bulked segregant analysis and genetic complementation defined *rgs1*^{cer7} as the allele responsible for constitutive expression of Mep2-GFP in conidia. (***A***) Micrographs showing expression of Mep2-GFP in segregating ascospores obtained from a cross between *cer7* and TH3. A single ascospore was isolated from an ascus under the dissecting microscope. Progeny displaying a high level of fluorescence signal from Mep2-GFP (*cer7*) were pooled together for whole genome sequencing. (Scale bar, 2 µm). Boxplots showing log2 values of fluorescence intensities of Mep2-GFP measured from conidia of 253 individual *M. oryzae* progeny. Progeny with *cer7* phenotype (blue), and those showing *CER7* phenotype (red), were compared to wild-type Guy11 conidia (black). n(*cer7*) =59, n(*CER7*) =194. A t-test was performed to determine the significance between the samples and *P* values are shown. (***B***) Graph showing SNP co-segregation frequencies on chromosome 2 after sequencing genomic DNA from pools of progeny segregating for *cer7* and *CER7* phenotypes, respectively. Red line shows frequencies of variants identified from pooled genomic DNA from progeny showing the *cer7* phenotype. Blue line shows frequencies of variants identified from pooled genomic DNA from progeny with *CER7* phenotype (***C***) Boxplot and micrographs to show the fluorescence intensity of Mep2-GFP in conidia of wild-type Guy11 (Black), *cer7* (red), Guy11:*rgs1*^{cer7} (blue), *cer7:RGS1*^{WT} (orange), Guy11::*rgs1*^{cer7} (grey), and *Δrgs1* (green). Letters within each sample refer to One-way ANOVA tests ($p<0.05$, Duncan test). Micrographs show bright field and epifluorescence images of conidia. (Scale bar, 10 µm).

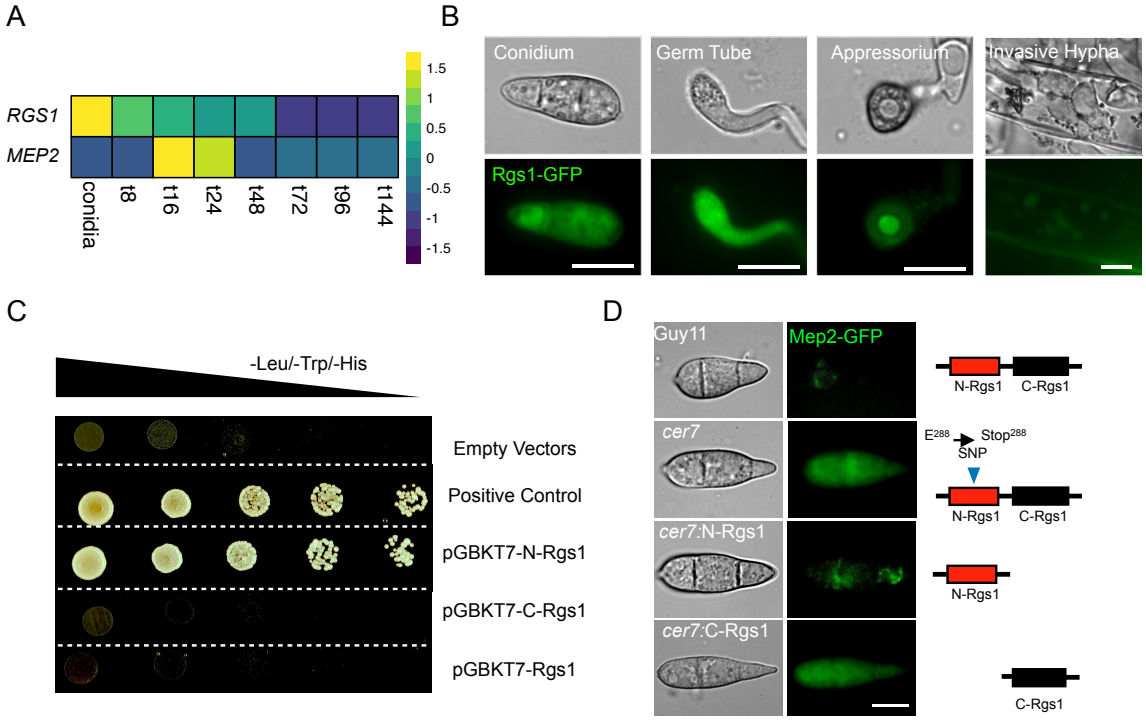

Figure 3. The N-terminus of N-Rgs1 is required for the repression of *MEP2* expression in conidia. ***A***) Heatmap showing relative transcript abundance of *MEP2* (MGG_00230) and *RGS1* (MGG_14517) genes in *M. oryzae* conidia, and during infection from 8 to 144 hpi. Relative transcript levels are fold change compared to expression in mycelium (from data set PRJEB44745). Data were extracted from RNA-seq dataset PRJEB45007. The colour key shows scaled fold change values. (***B***) Micrograph showing the fluorescence signal of Rgs1-GFP expressed in Guy11. Live-cell imaging was performed during a time course experiment to investigate expression of Rgs1-GFP in conidia, germ tubes, mature appressoria, and invasive hyphae at 24hpi. (***C***) Images showing transactivation activity of N-terminal Rgs1 (N-Rgs1), C-terminal Rgs1 (C-Rgs1), and full length Rgs1 in yeast cells. Co-transformation of Y2HGold yeast cells with bait (BD) and prey (AD) vectors was carried out with following combinations; pGBKT7-N-Rgs1 / pGADT7, pGBKT7-C-Rgs1 / pGADT7, pGBKT7-Rgs1/ pGADT7, and positive control (pGBKT7-53 and pGADT7-T) along with empty vectors, and grown in double drop-out and quadruple-dropout media. Images represent two independent biological replicates. (***D***) Micrographs showing expression of Mep2-GFP in conidia of strains *cer7*, Guy11, *cer7*:N-Rgs1, *cer7*:C-Rgs1. Conidia from each strain were harvested from colonies after 5 days growth on CM and immediately mounted on microscope slides for GFP visualization using epifluorescence microscopy. (Scale bar, 10 µm). The schematic illustration demonstrates different genotypes in corresponding *M. oryzae* strains.

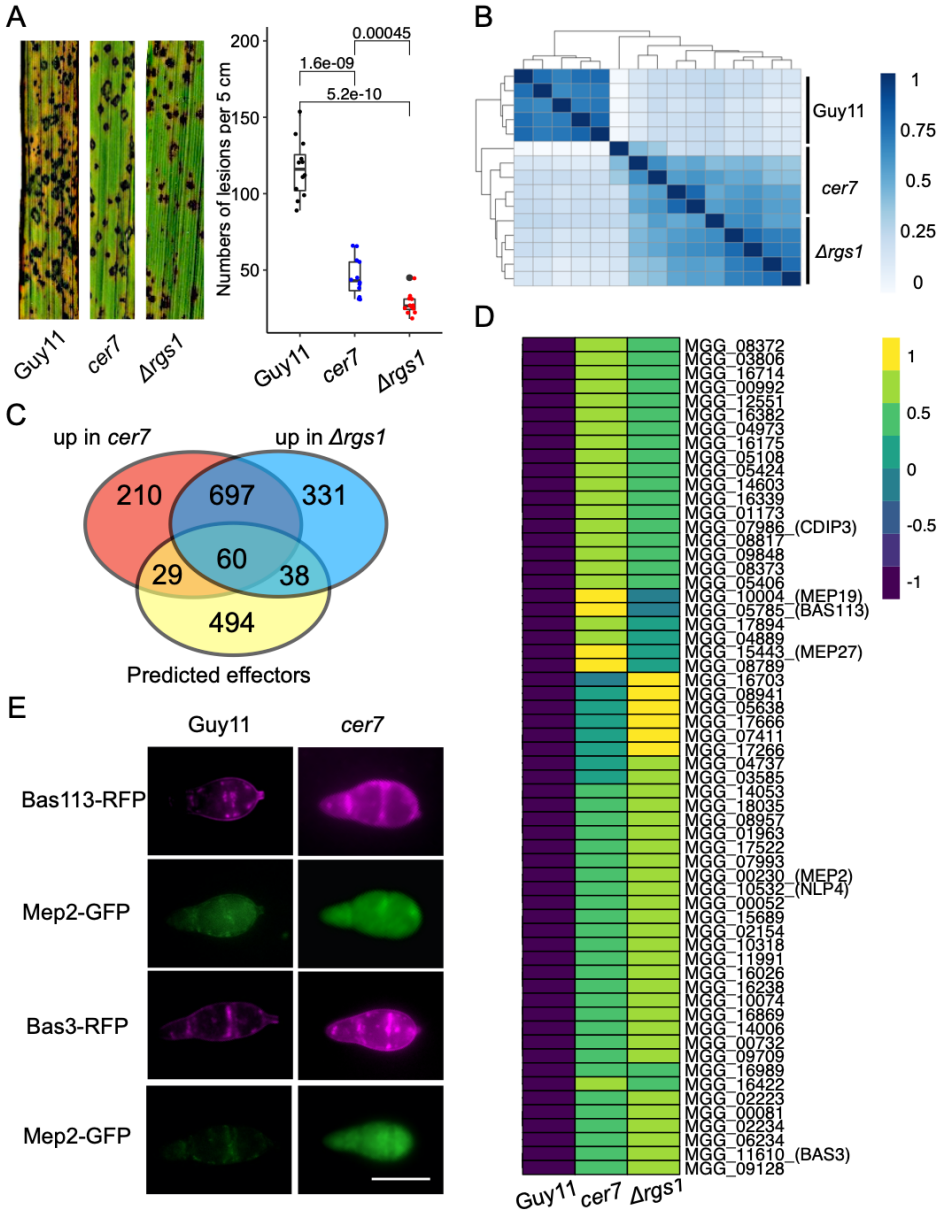

Figure 4. Rgs1 Regulates expression of a sub-population of effectors during plant infection. (***A***) Seedlings of rice cultivar CO-39 were inoculated with *M. oryzae* conidial suspensions of equal concentration (1 × 10^5 conidia/mL) of wild-type Guy11, *cer7* and *Δrgs1* mutants. The boxplot represents the number of rice blast disease lesions per 5 cm in three independent repetitions of the experiment. Unpaired Student's t-test was performed to determine significant differences. (***B***) Heatmap showing the Euclidean distance between RNA-seq samples from conidia of *cer7*, the wild type Guy11, and *Δrgs1*. Normalized reads counts were used from all the samples to determine clustering. Intensity of colours represent similarities and distance between samples. (***C)*** Venn diagram to show the number of effector genes de-repressed in conidia of the *cer7* and *Δrgs1* mutants. Blue circle = *cer7*, red circle =*Δrgs1*. (**D**) Heatmap showing expression of 60 effector genes significantly upregulated in conidia of *cer7* and *Δrgs1* mutants, compared to Guy11. Normalized expression values of transcripts used the TMM method. (***E***) Micrographs showing expression of Mep2-GFP, Bas113-RFP, and Bas3-RFP in conidia of *cer7* compared to Guy11. Conidial suspensions from each strain were inoculated onto hydrophobic glass coverslips and imaged using epifluorescence microscopy. (Scale bar, 10 μm).

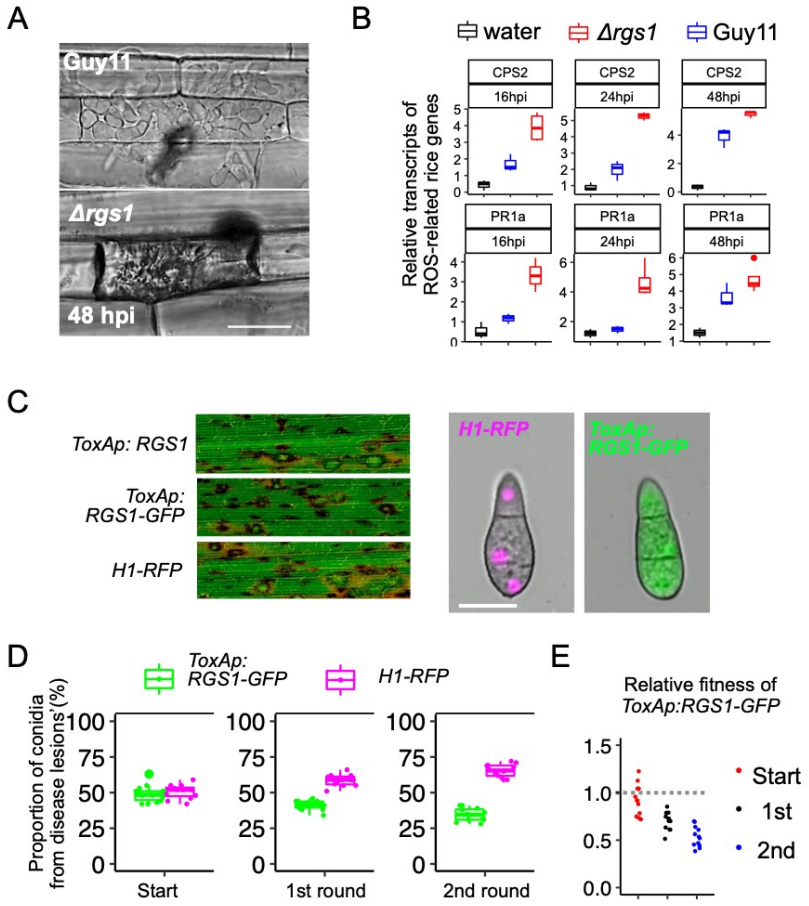

Figure 5. Rgs1 prevents rice defence gene expression and is a fitness determinant for rice blast disease. (***A***) Micrographs showing growth of invasive hyphae of Guy11 and *Δrgs1* 48hpi. (Scale bar, 10 µm). Rice leaf sheaths of rice cultivar CO39 were inoculated with conidial suspensions of Guy11 and *Δrgs1*. (Scale bars,12 µm). (***B***) Boxplots to show fold change values as relative transcripts of defence-related genes *CPS2* and *PR1a* in rice. Rice leaf sheath samples were inoculated with 0.02% gelatin (black), conidial suspension of Guy11 (blue) and *Δrgs1* (red). The qRT-PCR was performed using rice housekeeping genes eEF1A and UBQ5 as standards. (***C***) Seedlings of rice cultivar CO-39 were inoculated with conidial suspensions of equal concentration (1×10^5 conidia/mL) of *ToxAp:RGS1*, *ToxAp:RGS1-GFP* and Guy11:H1-RFP. Micrographs show representative images of blast disease symptoms of each strain. Conidia were harvested from colonies after 5 days growth on CM and immediately mounted on microscope slides for GFP visualization using epifluorescence microscopy. (Scale bar, 10 µm). (***D***). Boxplots showing the number of spores recovered from disease lesions following mixed infections with conidial suspensions of *H1-RFP* and *ToxAp:RGS1-GFP*. After 7 days, spores were collected from disease lesions, the ratio of each genotype determined and then used for subsequent inoculation of CO-39 seedlings. (***E***). The relative fitness of *ToxAp:Rgs1-GFP* was carried out using the formula: Relative fitness = $x_2(1-x_1) / x_1 (1-x_2)$, where x_1 is the initial frequency and x_2 the final frequency.

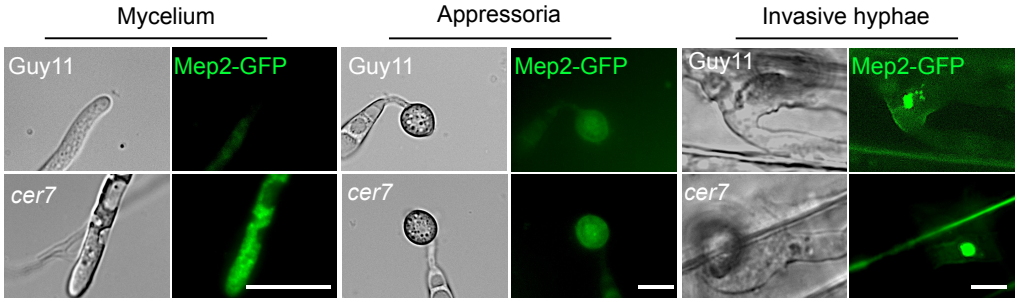

Fig. S1. Expression of Mep2-GFP in the *cer7* mutant strain is constitutively activated during different development stages including mycelium, appressoria, and invasive hyphae. Micrographs showing fluorescence of Mep2-GFP in Guy11 and the *cer7* mutant, in mycelium, appressoria, and invasive hyphae. Mycelium was imaged after 24 hours growing in liquid CM culture. The image for appressorium development was captured 8hpi on a hydrophobic glass coverslip. Invasive hyphae were imaged 32hpi on CO39 rice leaf sheath inoculated with conidial suspensions at $1x10^4$/mL (Scale bar, 10 μm).

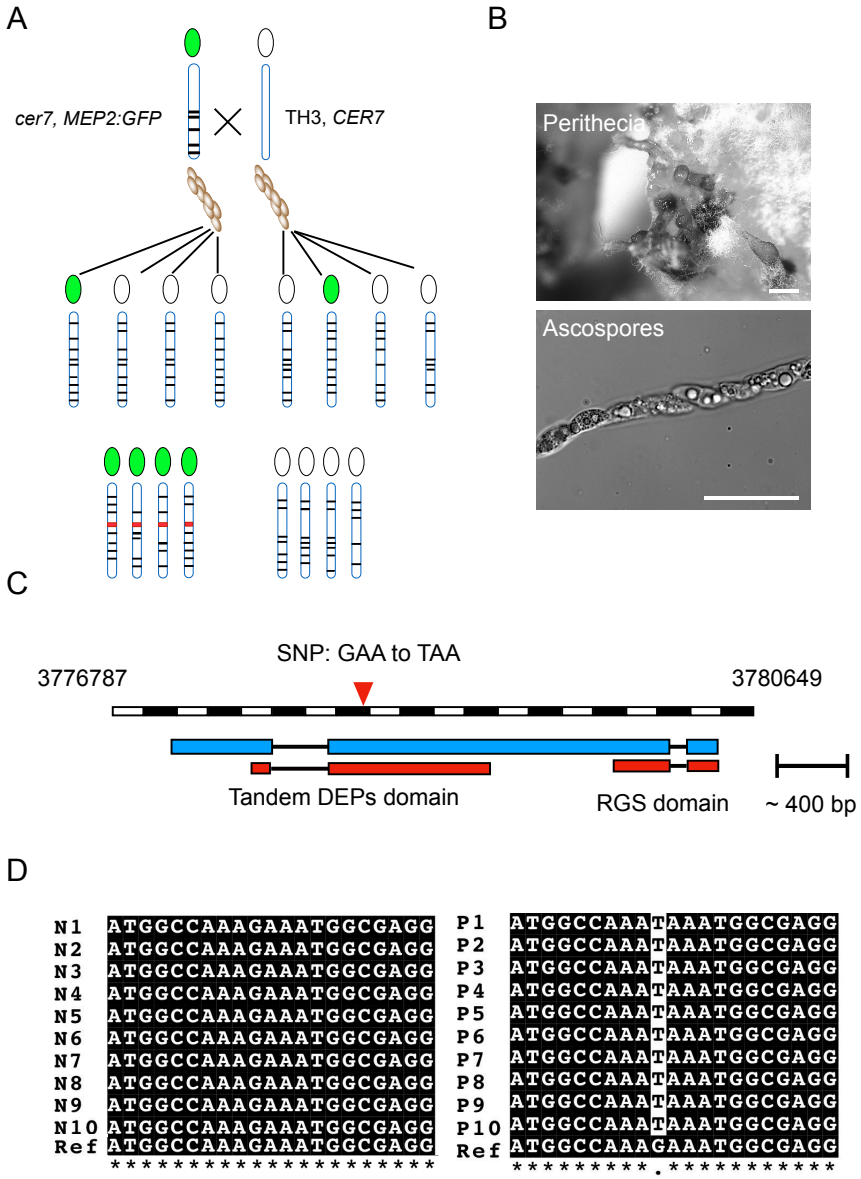

Fig. S2. Bulk segregant analysis defined a region of chromosome 2 showing very strong linkage to *cer7*. (***A***) Diagram to show bulked segregation analysis strategy to identify the mutant allele causing constitutive expression of *MEP2* in conidia. The *cer7* mutant (*Mat1-2*) and TH3 (*Mat1-1*) were used in sexual crosses by incubation together on oatmeal agar. After 4-6 weeks, perithecia developed and were collected and manipulated to release asci containing ascospore progeny. (***B***) Micrographs to show the perithecia and eight-spored ascus obtained from crossing *cer7* strain and TH3. (Scale bar, 10 μm). Images were captured after 8 weeks growth on oatmeal agar. (***C***) Overview of the genomic region of the *RGS1* locus to show transcript structures, and location of detected SNP in the highest linkage region identified by BSA. (***D***) Sequence analysis of amplicons of the *RGS1* coding sequences from 20 ascospore progeny. N1 to N10 are amplicons from progeny showing low Mep2-GFP fluorescence (wild-type), and P1 to P10 represent amplicons of progeny showing high expression of Mep2-GFP (*cer7*). “Ref” shows the DNA sequence of *RGS1* in the *M. oryzae* reference genome.

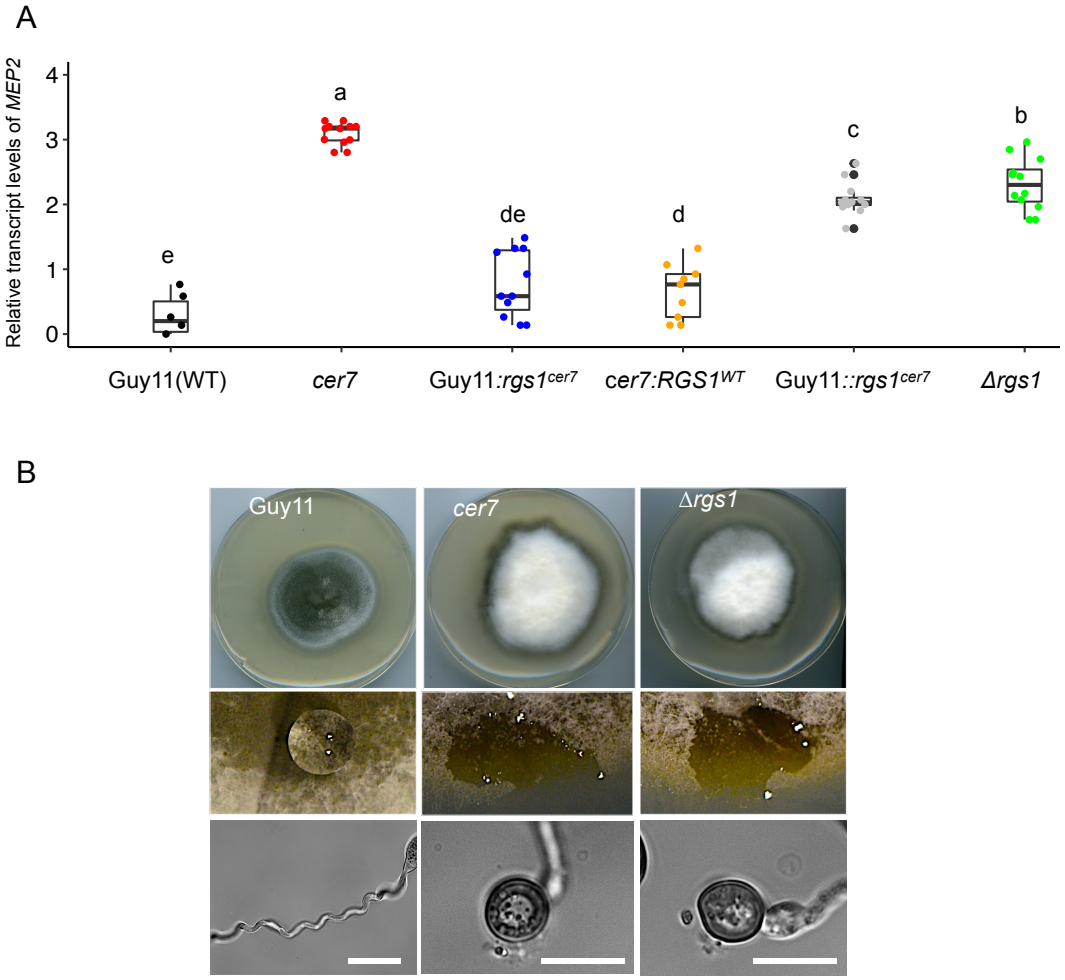

Fig. S3. Complementation analysis of the *cer7* mutant with *RGS1*. (***A***) Box plot to show fold change in relative transcripts of *MEP2* from mycelium of the wild type Guy11 (Black), *cer7* mutant (red), Guy11:*rgs1*^{cer7} ectopic transformant (blue), *cer7:RGS1*^{WT} complemented transformant (orange), Guy11::*rgs1*^{cer7} allelic replacement mutant (grey) *Δrgs1* mutant (green). Expression was determined relative to the fungal actin gene. Letters refer to significant differences determined by One-way ANOVA tests ($p<0.05$, Duncan test). (***B***) Upper panel Images to show the colony morphology of wild type Guy11, compared to *cer7* and Δ*rgs1* mutants. Both *cer7* and Δ*rgs1* form white fluffy colonies when grown on complete medium. Mid panel images show droplets of water placed on the surface of plate cultures of Guy11, *cer7* and Δ*rgs1* mutant strains. Mutants show an easily-wettable phenotype. Photographs were taken 24hpi. Lower panel micrographs show appressorium development by *cer7* and Δ*rgs1* mutants on a non-inductive hydrophilic surface. (Scale bar, 10 μm).

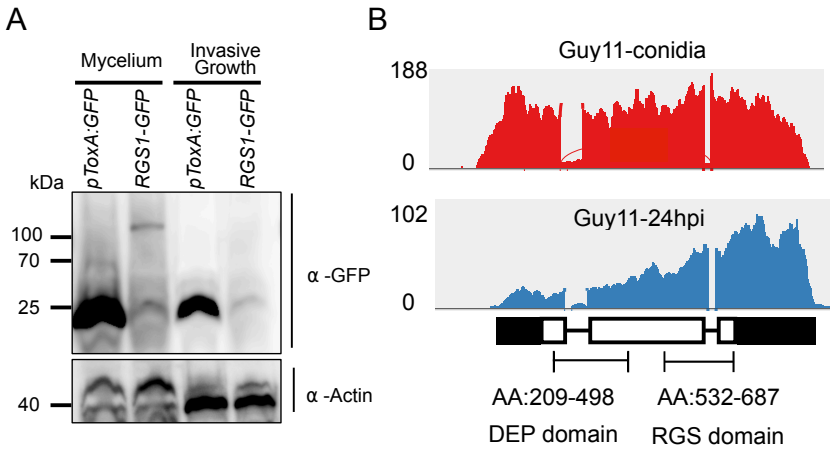

Figure S4. Expression analysis of *RGS1*. (***A***) Western blot showing abundance of Rgs1-GFP detected with anti-GFP antibody in mycelium and invasive hyphae (IH). Total protein extracted from mycelium of Rgs1-GFP after growing in liquid CM culture for 48 hours. Lysates were resolved by SDS-PAGE and analysed by western blot using antibodies against GFP. Detection using anti-actin was used as the loading control for fungal protein. Molecular mass standards in kDa are indicated on the left. (***B***) Sashimi plots showing mRNA transcript reads of *RGS1* in Guy11, as conidia at 0hpi (red), and during infection at 24hpi (blue). The bar plot demonstrated the depth of reads aligned to corresponding regions of the gene. RNA-seq from libraries of total RNA isolated from leaf-drop infection inoculated by wild-type Guy11 were used. The numbers on the left panel indicate the coverage of reads detected after alignment and visualized in IGV.

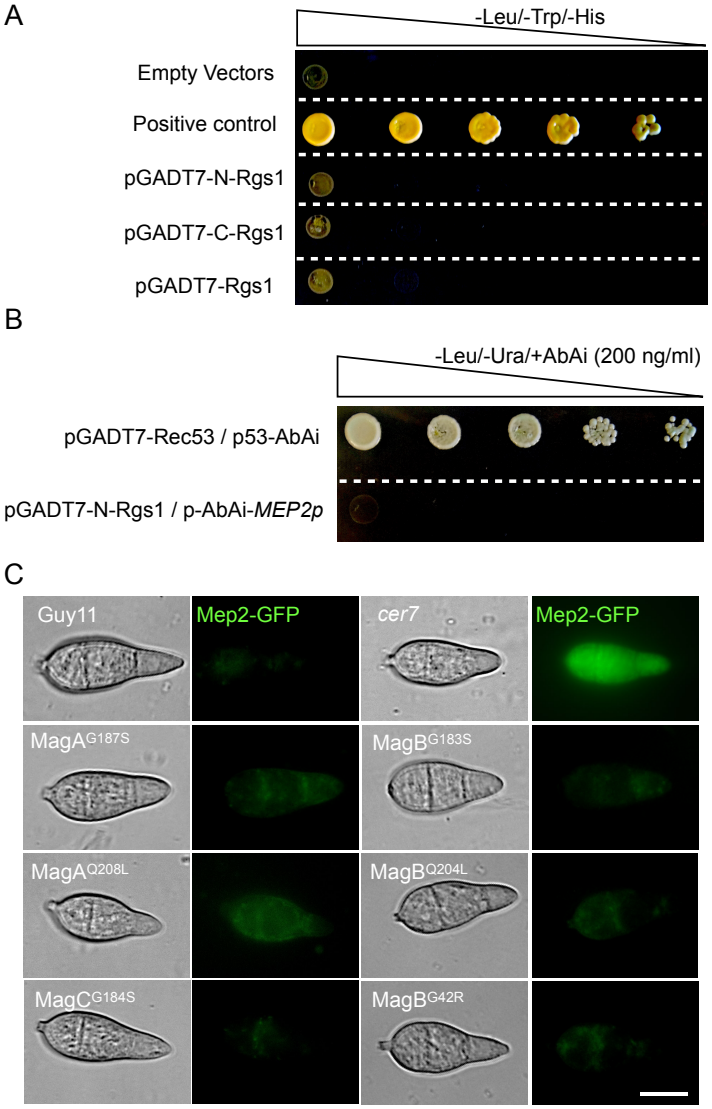

Fig. S5. N-Rgs1 does not possess DNA-binding ability or bind to the *MEP2* promoter. (***A***) DNA-binding assay of N-Rgs1, C-Rgs1, and full length Rgs1 in yeast cells. Co-transformation of Y2HGold strains was carried out with bait (BD) and prey (AD) vectors in the following combinations; pGBKT7 / pGADT7-N-Rgs1, pGBKT7 / pGADT7-C-Rgs1, pGBKT7 / pGADT7-Rgs1, and positive control (pGBKT7-53 and pGADT7-T) along with empty vectors. Cells were grown on double drop out quadruple dropout medium. Images are representative of two biological replicates. (***B***) Yeast-one-hybrid assay to determine the interaction between Rgs1 and upstream sequences of the *MEP2* gene. The Y1HGold strain containing p-AbAi-*MEP2p* was transformed by introducing plasmid pGADT7-Rgs1$^{1-498}$ and used to test growth on medium with -Leu/-Ura, supplemented with 200 ng/mL Aureobasidin A (AbA). (***C***) The repression of *MEP2* expression by Rgs1 occurs in a G-protein signalling-independent manner. Micrographs showing expression of Mep2-GFP in conidia of Guy11, *cer7*, MagA^{G187S}, MagB^{G183S}, MagA^{Q208L}, MagB^{Q204L}, MagC^{G184S}, and MagB^{G42R}. MagA^{G187S}, MagB^{G183S}, and MagC^{G184S}. Images are representative at least 10 transformants examined for each experiment. Conidial suspensions from each strain were harvested from colonies after 5 days growth on CM and immediately visualized using epifluorescence microscopy. (Scale bar, 10 μm).

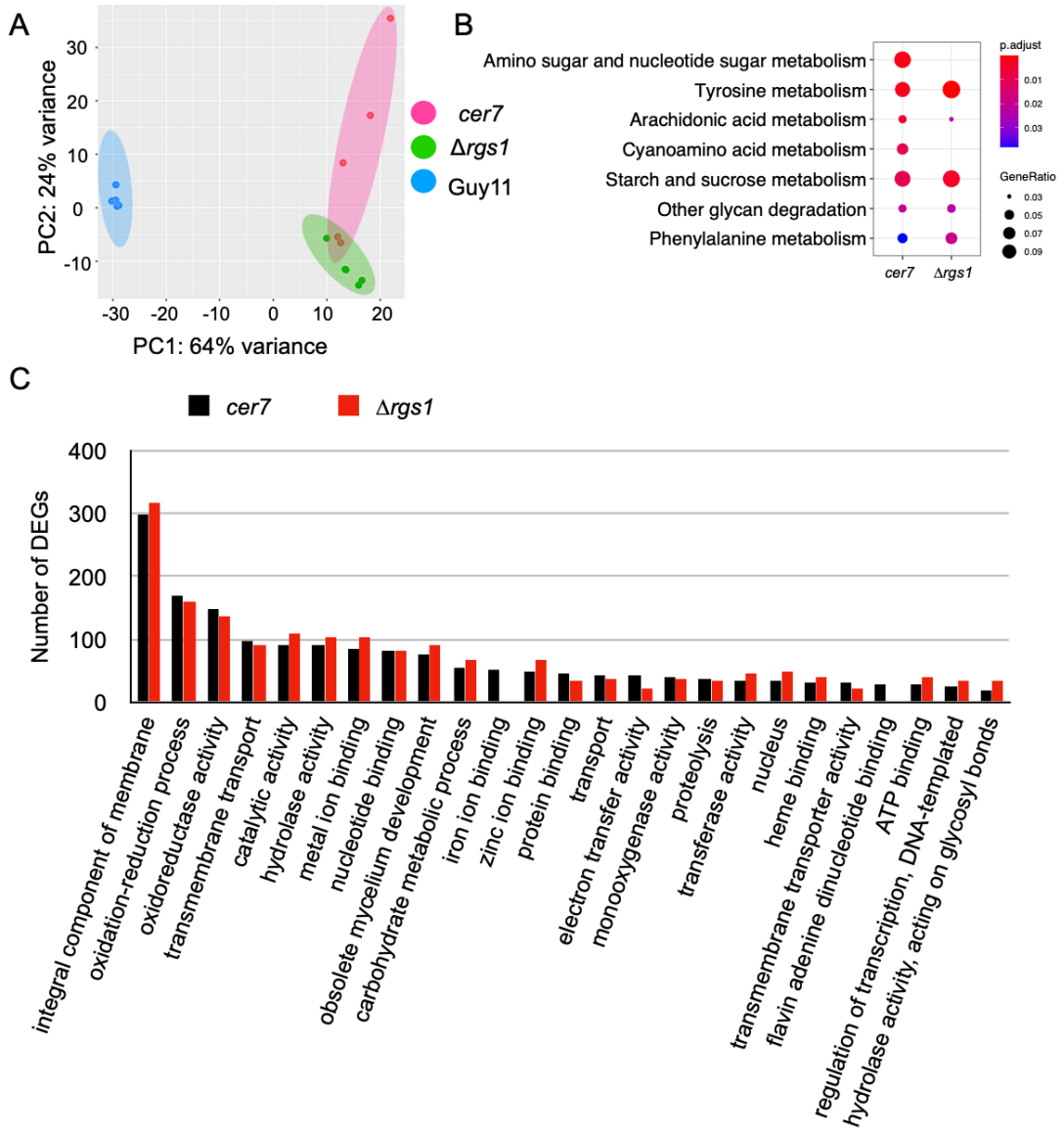

Fig. S6. RNA-seq analysis of *cer7*, *Δrgs1* and Guy11. (***A***) Plot showing Principal Component Analysis (PCA) to determine the distance between samples analysed by RNA-seq. Genes with raw reads counts of less than 10 were discarded, and remaining read counts normalized as FPKMs and used to perform analysis to generate Principal Components (PCs). The x-axis shows PC1, and the y-axis show PC2. Red dots represent samples from the *cer7* mutant, blue dots represent Guy11, and green dots represent the Δ*rgs1* mutant. (***B***) Dot plot showing the comparative metabolic pathway enrichment analysis of DEGs identified from RNA-seq of *cer7* and Δ*rgs1*. The size of dots indicates the ratio of the number of DEGs in the pathway / the number of total DEGs. (***C***) Bar chart showing the top 25 biological processes enriched in DEGs in *cer7* and *Δrgs1* mutants compared to Guy11, based on Gene Ontology analysis of RNA-seq data. The X-axis shows corresponding functions according to the Gene Ontology annotation of *M. oryzae*. The Y-axis shows the number of DEGs identified from the RNA-seq dataset. Black bar plots represent the comparison between *cer7* and Guy11. Red bar plots represent comparison between *Δrgs1* and Guy11.

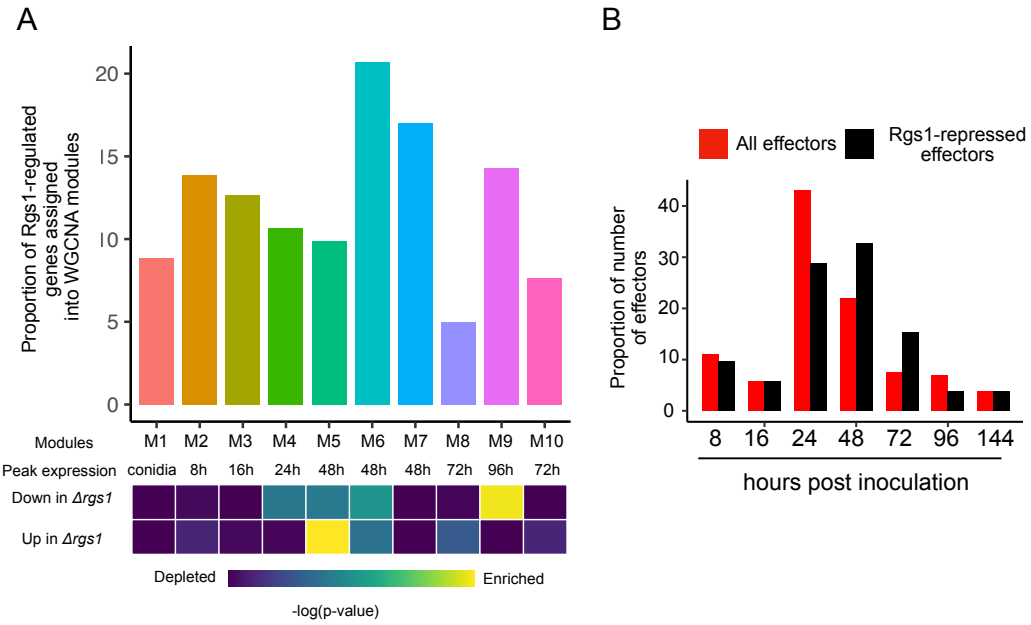

Fig. S7 Rgs1-regulated effectors temporally co-expressed during plant infection. (***A***) Bar chart to show the fraction of Rgs1-regulated genes assigned to each WCGNA co-expression module defined in Ref. 1. X-axis shows the time-point of peak expression during plant infection as described previously (25). The heatmap shows enrichment of Rgs1-regulated genes. Enrichment of genes up-regulated in *Δrgs1* conidia was observed in WCGNA modules M4, M5 and M6 which show peak expression at 24-48hpi. Genes down-regulated in *Δrgs1* conidia was observed in M9, which peaks in expression at 96hpi. (***B***). Bar chart to show temporal expression profiles of *M. oryzae* effector-encoding genes (25). Black bars indicate the number of Rgs1-regulated effectors, and red bars the total number of putative effectors expressed at each time point. Rgs1-regulated effectors are over-represented among those peaking in expression at 24h and 48h, consistent with WCGNA co-expression analysis.

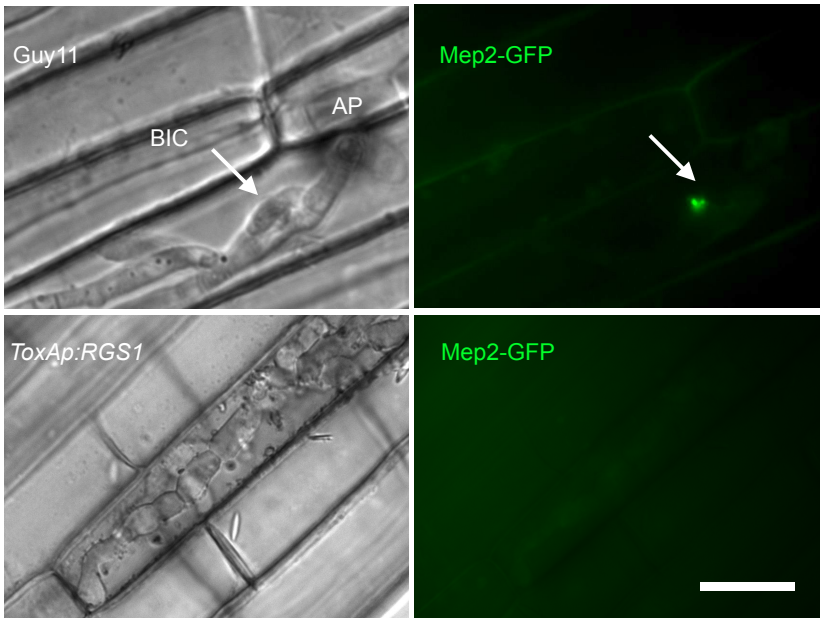

Fig. S8. Constitutive Rgs1 over-expression prevents Mep2-GFP expression *in planta*. Micrographs to show expression of Mep2-GFP in the BIC of invasive hyphae of Guy11 and the *ToxAp:RGS1* strain which constitutively expresses *RGS1*. BIC localization was imaged in rice leaf sheath tissue inoculated by conidia of Guy11:Mep2-GFP at 32 hpi. (Scale bar, 10 μm).

Table S1. **Primers used in this study**

Primer name	Sequence (5'-3')	length (bases)
MEP2p-F	CGCGGTGGCGGCCGCTCTAGAGGTACAGGAGGAAGAAGATACA	43
Mep2-R-GFP	GCCCTTGCTCACCATTATGTCAAACCGAACAGGAGGA	37
Rgs1 -F	TGCAGCCCAATGTGGAATTCCTTGGTATGGCCAGAATCGACA	43
Rgs1 -R	TCGACGGTATCGATAAGCTTAGTACGTAACAATCTCGTCTACGA	45
Rgs1-native-allele-P1	CTCGCTCAAGTTCTCCCAGTCAA	24
Rgs1-native-allele-P2	GTCGTGACTGGGAAAACCCTGGCGGTCTGATGAACGAATGACTTGAAG	49
Rgs1-native-allele-P3	TCCTGTGTGAAATTGTTATCCGCTCTACAATATACACCAGGTCTGCCAA	50
Rgs1-native-allele-P4	GGCTTGAGTCAAATGGAATTCG	23
M13F	CGCCAGGGTTTTCCCAGTCACGAC	25
M13R	AGCGGATAACAATTTCACACAGGA	25
Hysplit	GGATGCCTCCGCTCGAAGTA	21
Ygsplit	CGTTGCAAGACCTGCCTGAA	21
Rgs1-KO-1	AGGCGCTATACCCCTTACTGTT	23
Rgs1-KO-2	GTCGTGACTGGGAAAACCCTGGCGAAGCTGAGGGTCTTTCCTTGGA	47
Rgs1-KO-3	TCCTGTGTGAAATTGTTATCCGCTGCATTGTCTTGGTGATGTTTATT	48
Rgs1-KO-4	AATGAGTGACGACCTTGATGT	22
BAS113p-F	TGCAGCCCAATGTGGAATTCAACAATCCCTACCACGTAGCA	42
BAS113-RFP-R	GCCCTTGCTCACCATCCATCCGTTCCACCAGGTGT	36
RFP-F	ATGGTGAGCAAGGGCGA	18
RFP-R	TCGACGGTATCGATAAGCTTCCCTCGAGTGGAGATGTGGAGT	43
Rgs1-GFP-F	CGCGGTGGCGGCCGCTCTAGAGCACACATCATAAAGAAACG	41
Rgs1-GFP-R	TCGACGGTATCGATAAGCTTCGTTGCGAGCGGCTTTGG	38
N-Rgs1-F	TGCAGCCCAATGTGGAATTCGCACACATCATAAAGAAACG	40
N-Rgs1-R	TCGACGGTATCGATAAGCTTGTTGATCATGTCCTTGCCTTTAC	43
C-Rgs1-F	TGCAGCCCAATGTGGAATTCATGGGCTCAGTCCCCAGGG	39
C-Rgs1-R	TCGACGGTATCGATAAGCTTAGTACGTAACAATCTCGTCTACGA	45
RGS1_pGBKT7_F	CATGGAGGCCGAATTCATGGACGACACCTCCCG	34
RGS1_pGBKT7_R	GCAGGTCGACGGATCCTAACCGTTGCGAGCGGCT	35
N-Rgs1-pGBKT7-F	CATGGAGGCCGAATTCATGGACTTTAAGGATTTGTTCGCTAC	43
N-Rgs1-pGBKT7-R	GCAGGTCGACGGATCCTAATTAGTTGATCATGTCCTTGCCTTTAC	45
C-Rgs1-pGBKT7-F	CATGGAGGCCGAATTCATGCCAAATGTCAAGTCTAGCGTCA	42
C-Rgs1-pGBKT7-R	GCAGGTCGACGGATCCTAAGATCATGTCCTTGCCTTTACTTG	43
RGS1_pGBGT7_F	ATGGCCATGGAGGCCAGTATGGACGACACCTCCCG	36
RGS1_pGBGT7_R	AGCTCGAGCTCGATGAACCGTTGCGAGCGGCT	33
N-Rgs1-pGBGT7-F	ATGGCCATGGAGGCCAGTATGGACTTTAAGGATTTGTTCGCTAC	45
N-Rgs1-pGBGT7-R	AGCTCGAGCTCGATGTAATTAGTTGATCATGTCCTTGCCTTTAC	44
C-Rgs1-pGBGT7-F	ATGGCCATGGAGGCCAGTATGCCAAATGTCAAGTCTAGCGTCA	44
C-Rgs1-pGBGT7-R	AGCTCGAGCTCGATGTAAGATCATGTCCTTGCCTTTACTTG	42
MEP2-promoter-F	AAATGATGAATTGAAAAGCTTTCCTCCTGTTCGGTTTGACA	41
MEP2-promoter-R	ATACAGAGCACATGCCTCGAGCATTTAGCTGAGCTTGGTC	40
Rgs1-cDNA-F	GCCATGGAGGCCAGTGAATTCATGGACGACACCTCCCG	38
Rgs1-cDNA-R	ACGATTCATCTGCAGCTCGAGTAACCGTTGCGAGCGGCT	39
MagA-G187S-p1	TGCAGCCCAATGTGGAATTCATCTCGACGAATACCATGCGT	41
MagA-G187S-p2	GCTTGTAGTTTTTGTTCTTGC	21
MagA-G187S-p3	ACAAAAACTACAAGCATATACGA	23
MagA-G187S-p4	TCGACGGTATCGATAAGCTTTCGTCGTGCGATCTCTGC	38

MagA-Q208L-p1	TGCAGCCCAATGTGGAATTCATCTCGACGAATACCATGCGT	41
MagA-Q208L-p2	CCTGCTGCCTCCTACATCAAA	21
MagA-Q208L-p3	GTAGGAGGCAGCAGGAGTGAGC	22
MagA-Q208L-p4	TCGACGGTATCGATAAGCTTTCGTCGTGCGATCTCTGC	38
MagB-G183S-p1	TGCAGCCCAATGTGGAATTCCATCTATCAAAGCAAGTCGCCA	42
MagB-G183S-p2	CTCAGTGATACTGGTTGTCTTG	22
MagB-G183S-p3	ACCAGTATCACTGAGACGACTT	22
MagB-G183S-p4	TCGACGGTATCGATAAGCTTTGCCTGGTGTAATTCGGCT	39
MagB-Q204L-p1	TGCAGCCCAATGTGGAATTCCATCTATCAAAGCAAGTCGCCA	42
MagB-Q204L-p2	GAACGGCTGCCACCAACATC	20
MagB-Q204L-p3	TGGTGGCAGCCGTTCTGAGC	20
MagB-Q204L-p4	TCGACGGTATCGATAAGCTTTGCCTGGTGTAATTCGGCT	39
MagB-G42R-p1	TGCAGCCCAATGTGGAATTCCATCTATCAAAGCAAGTCGCCA	42
MagB-G42R-p2	TTCACGGGCTCCGAGCAGAA	20
MagB-G42R-p3	CTCGGAGCCCGTGAATCCG	19
MagB-G42R-p4	TCGACGGTATCGATAAGCTTTGCCTGGTGTAATTCGGCT	39
MagC-G184s-p1	TGCAGCCCAATGTGGAATTCTACCCACCTTGTCCACCTT	39
MagC-G184s-p2	GCACATCTTGCCAGAGaGCAATTGGCGGATTGCTCC	36
MagC-G184s-p3	GGAGCAATCCGCCAATTGCCCTCTGGCAAGATGTGC	36
MagC-G184s-p4	TCGACGGTATCGATAAGCTTAGCCTCCACTGGAACTAGCCC	41
BAS3p-F	TGCAGCCCAATGTGGAATTCCATCTGCAGCGACGATCTGT	40
BAS3-RFP-R	GCCCTTGCTCACCATCTGGGCACTGTTGGCAGCG	34
N-Rgs1_p1	TGCAGCCCAATGTGGAATTC GCACACATCATAAAGAAACG	41
N-Rgs1_p2	GTTGATCATGTCCTTGCCTT	20
N-Rgs1_p3	AAGGACATGATCAACTGAAATTAATCCAGCC	31
N-Rgs1_p4	TCGACGGTATCGATAAGCTTGGCTTGAGTCAAATGGAATTCG	42
C-Rgs1_p1	TGCAGCCCAATGTGGAATTCGCACACATCATAAAGAAACG	40
C-Rgs1_p2	CTACCACCGAACAAAAGCTGAG	22
C-Rgs1_p3	TTTTGTTCGGTGGTAGATGGGCTCAGTCCCCAGG	34
C-Rgs1_p4	GACGGTATCGATAAGCTTGGCTTGAGTCAAATGGAATTCG	40
MEP2-F	TTAGCCCTTGCTGCTGC	17
MEP2-R	TTGGCTTCACCAAACG	16
Mo-actin-F	GTGACTTGACCGACTACCTGA	22
Mo-actin-R	TGCCGATGGTGATAACCTGT	21
β-tubulin-F	CTGCCATCTTCCGTGGAAAGG	22
β-tubulin-R	GACGAAGTACGACGAGTTCTTG	23
PR1a-F	TGGGTGTCGGAGAAGCAGTG	24
PR1a-R	GGTGATGAAGACGCCGAGG	20
PR10b-F	ATGTTACTGTGGCGTGGTCGCATGT	31
PR10b-R	TGTGTATTTTATTCACTCGTGAAGCA	27
CPS2-F	CAATCGAGATCTGCTCAGGA	26
CPS2-R	CTGGCGTAGTCTGCACTGTT	21
Rice-AK061464-F	TTTCACTCTTGGTGTGAAGCAGAT	24
Rice-AK061464-R	GACTTCCTTCACGATTTCATCGTAA	25
Rice-AK061988-F	ACCACTTCGACCGCCACTACT	21
Rice-AK061988-R	ACGCCTAAGCCTGCTGGTT	19

Table S2 *Magnaporthe oryzae* strains generated in this study

Strain Name	Description
cer7	Guy11 constitutively expressing Mep2-GFP after UV mutagenesis
Mep2-GFP	Guy11 transformed with plasmid pMep2-GFP
cer7/Rgs1cer7	Cer7 transformed with plasmid Rgs1cer7
cer7/Rgs1wt	Cer7 transformed with plasmid RGs1wt
Δrgs1	targeted gene deletion in Rgs1 locus
Rgs1CER7	Guy11 transformed with plasmid pMep2-GFP and transformated with native allele of Rgs1 carrying the Cer7 mutant
Δrgs1/Mep2-GFP	Δrgs1 transformed with plasmid pMep2-GFP
Mep2-GFP/rgs1cer7	Guy11 strain with Mep2-GFP and transformed with plasmid rgs1cer7
pToxA-GFP	Guy11 with constituveily expressed GFP driven by pToxA
Rgs1-GFP	Guy11 transformed with plasmid Rgs1-GFP
cer7/N-Rgs1	Cer7 transformed with plasmid N-Rgs1
cer7/C-Rgs1	Cer7 transformed with plasmid C-Rgs1
MagA-Q208L	Guy11 constitutively expressing Mep2-GFP and transformed with plasmid MagA-Q208L
MagA-G187S	Guy11 constitutively expressing Mep2-GFP and transformed with plasmid MagA-G187S
MagB-G183S	Guy11 constitutively expressing Mep2-GFP and transformed with plasmid MagB-G183S
MagB-Q204L	Guy11 constitutively expressing Mep2-GFP and transformed with plasmid MagB-Q204L
MagB-G42R	Guy11 constitutively expressing Mep2-GFP and transformed with plasmid MagA-Q208L
MagC-G184S	Guy11 constitutively expressing Mep2-GFP and transformed with plasmid MagC-G184S
Cer7/bas113-RFP	Cer7 transformed with plasmid Bas113-RFP
Cer7/Bas3-RFP	Cer7 transformed with plasmid Bas3-RFP
pToxA-Rgs1-GFP	Guy11 transformed with plasmid pToxA-Rgs1-GFP

Table S3 Rgs1-regulated effectors identified in this study

Gene Locus Number	Gene Name	Reference
MGG_07986	CDIP3	Chen, Songbiao, Pattavipha Songkumarn, R. C. Venu, Malali Gowda, Maria Bellizzi, Jinnan Hu, Wende Liu et al. "Identification and characterization of in planta–expressed secreted effector proteins from *Magnaporthe oryzae* that induce cell death in rice." *Molecular plant-microbe interactions* 26, no. 2 (2013): 191-202.
MGG_10532	NLP4	Fang, Ya-Li, You-Liang Peng, and Jun Fan. "The Nep1-like protein family of *Magnaporthe oryzae* is dispensable for the infection of rice plants." *Scientific reports* 7, no. 1 (2017): 1-10.
MGG_05785	BAS113	Giraldo, Martha C., Yasin F. Dagdas, Yogesh K. Gupta, Thomas A. Mentlak, Mihwa Yi, Ana Lilia Martinez-Rocha, Hiromasa Saitoh, Ryohei Terauchi, Nicholas J. Talbot, and Barbara Valent. "Two distinct secretion systems facilitate tissue invasion by the rice blast fungus *Magnaporthe oryzae*." *Nature communications* 4, no. 1 (2013): 1-12.
MGG_11610	BAS3	Mosquera, Gloria, Martha C. Giraldo, Chang Hyun Khang, Sean Coughlan, and Barbara Valent. "Interaction transcriptome analysis identifies *Magnaporthe oryzae* BAS1-4 as biotrophy-associated secreted proteins in rice blast disease." *The Plant Cell* 21, no. 4 (2009): 1273-1290.
MGG_02154	SPD5	Sharpee, William, Yeonyee Oh, Mihwa Yi, William Franck, Alex Eyre, Laura H. Okagaki, Barbara Valent, and Ralph A. Dean. "Identification and characterization of suppressors of plant cell death (SPD) effectors from *Magnaporthe oryzae*." *Molecular plant pathology* 18, no. 6 (2017): 850-863.
MGG_00230	MEP2	Yan, Xia, Bozeng Tang, Lauren Ryder, Dan Maclean, Vincent M. Were, Alice Bisola Eseola, Neftaly Cruz-Mireles, Andy Foster, Miriam Osés-Ruiz, and Nicholas J. Talbot. "The transcriptional landscape of plant infection by the rice blast fungus *Magnaporthe oryzae* reveals distinct families of temporally co-regulated and structurally conserved effectors." *bioRxiv* (2022).
MGG_15443	MEP27	Yan, Xia, Bozeng Tang, Lauren Ryder, Dan Maclean, Vincent M. Were, Alice Bisola Eseola, Neftaly Cruz-Mireles, Andy Foster, Miriam Osés-Ruiz, and Nicholas J. Talbot. "The transcriptional landscape of plant infection by the rice blast fungus *Magnaporthe oryzae* reveals distinct families of temporally co-regulated and structurally conserved effectors." *bioRxiv* (2022).
MGG_10004	MEP19	Yan, Xia, Bozeng Tang, Lauren Ryder, Dan Maclean, Vincent M. Were, Alice Bisola Eseola, Neftaly Cruz-Mireles, Andy Foster, Miriam Osés-Ruiz, and Nicholas J. Talbot. "The transcriptional landscape of plant infection by the rice blast fungus *Magnaporthe oryzae* reveals distinct families of temporally co-regulated and structurally conserved effectors." *bioRxiv* (2022).
MGG_14053		
MGG_16703		
MGG_10318		
MGG_10074		
MGG_07411		
MGG_08957		
MGG_08372		
MGG_12551		
MGG_16175		
MGG_00732		
MGG_08373		
MGG_16026		
MGG_00081		

MGG_18035
MGG_16989
MGG_08789
MGG_05424
MGG_16238
MGG_09848
MGG_06234
MGG_04737
MGG_17666
MGG_16869
MGG_14006
MGG_16714
MGG_03806
MGG_03585
MGG_02234
MGG_08941
MGG_08817
MGG_17266
MGG_05638
MGG_14603
MGG_00052
MGG_05406
MGG_09709
MGG_17522
MGG_17894
MGG_02223
MGG_15689
MGG_05108
MGG_16339
MGG_01963
MGG_16422
MGG_16382
MGG_07993
MGG_09128
MGG_01173
MGG_11991
MGG_04973
MGG_00992
MGG_04889